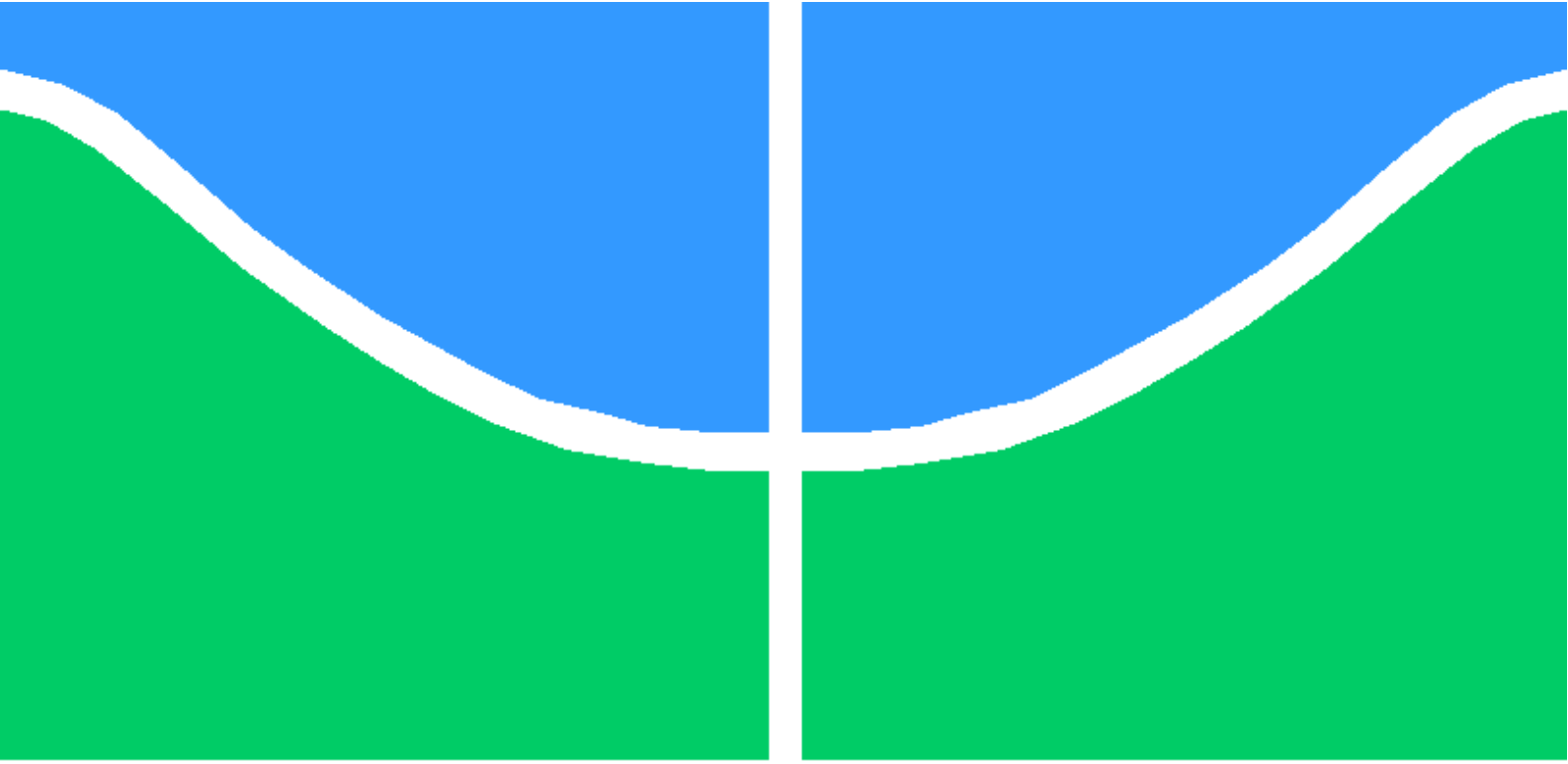

DIPLOMA THESIS

DIRECTION OF ARRIVAL ESTIMATION USING OFF-THE-SHELF DIRECTIONAL ANTENNAS ARRAY

Daniel Akira Ando

Brasilia, June 2018

UNIVERSITY OF BRASILIA

TECHNOLOGY FACULTY

UNIVERSITY OF BRASILIA
Technology College

DIPLOMA THESIS

DIRECTION OF ARRIVAL ESTIMATION USING OFF-THE-SHELF DIRECTIONAL ANTENNAS ARRAY

Daniel Akira Ando

Thesis submitted to the Electrical Engineering
Department in partial fulfilment of the
requirements to obtain the degree of Network Communication Engineer

Examining Committee

João Paulo Carvalho Lustosa da Costa, ENE/UnB _____
Advisor

Ricardo Kehrle Miranda, ENE/UnB _____
Co-advisor

Ricardo Zelenovsky, ENE/UnB _____
Examiner

Marco Antonio Marques Marinho, ENE/UnB _____
Examiner

FICHA CATALOGRÁFICA

ANDO, DANIEL AKIRA

DIRECTION OF ARRIVAL ESTIMATION VIA RECEIVED SIGNAL STRENGTH WITH OFF-THE-SHELF DIRECTIONAL ANTENNAS / Daniel Akira Ando; Orientador: João Paulo Carvalo Lustosa da Costa; Coorientador: Ricardo Kehrle Miranda. – [Distrito Federal] 2018.

x11, 42p., 210 x 297 mm (ENE/FT/UnB, Engenheiro de Redes de Comunicação, Engenharia de Redes de Comunicação, 2018).

Trabalho de Graduação – Universidade de Brasília, Faculdade de Tecnologia.

Departamento de Engenharia Elétrica

1. Direction of Arrival
2. Antenna Array
3. Directional Antenna
4. Software-Defined Radio
5. Unmanned Aerial Vehicle

I. ENE/FT/UnB

II. Título (série)

REFERÊNCIA BIBLIOGRÁFICA

ANDO, DANIEL AKIRA (2018). DIRECTION OF ARRIVAL ESTIMATION VIA RECEIVED SIGNAL STRENGTH WITH OFF-THE-SHELF DIRECTIONAL ANTENNAS, Projeto Final de Graduação em Engenharia de Redes de Comunicações, Publicação 2018, Departamento de Engenharia Elétrica, Universidade de Brasília, Brasília,DF, 42p.

CESSÃO DE DIREITOS

AUTORES: Daniel Akira Ando

TÍTULO: DIRECTION OF ARRIVAL ESTIMATION VIA RECEIVED SIGNAL STRENGTH WITH OFF-THE-SHELF DIRECTIONAL ANTENNAS

GRAU: Engenheiro de Redes de Comunicações ANO: 2018

Daniel Akira Ando
Departamento de Eng. Elétrica
Universidade de Brasília
Campus Darcy Ribeiro

Dedication

I dedicate this work to my parents, whose great support and love gave me strengths throughout my life

Daniel Akira Ando

Acknowledgments

Above all, I would like to thank my family. I am where I am because of their support, caring and understanding. I would like to especially thank my dad for being more than a father for me, but also the greatest of all friends and my source of inspiration. All my achievements are thanks to him, who believes in me even when I don't myself.
I would like to acknowledge the uninterrupted support, patience and guiding received from Ricardo Kehrle Miranda and Marcos Teixeira de Oliveira. I appreciated every day spent with them, for I have learned how to think like a scientist. They taught me the ways of becoming an engineering researcher and encouraged me for always pursuing my dreams.
I would also like to thank professor Jõao Paulo C. Lustosa da Costa for the great support and care for our team. Without him, nothing of these would have been possible.
Next, I would like to deeply thank Sensei Jorge Kishikawa and all the Instituto Cultural Niten's samurais for being my second family. Sensei Jorge Kishikawa is constantly teaching us the values of compassion, courage, honour, justice and bringing us together to the Japanese culture, which greatly influences my character. I also thank Niten Brasilia for sharing every single drop of sweat on the pursue of becoming better human beings.
Of course I can't possibly forget about all my friends who made the path until here pleasant and enjoyable. I won't ever forget the moments we spent together and I'm truly thankful for each one of you. Special thanks to Victor Patterson Zottmann, Ana Luiza Ferreira Veiga Barros, Clarissa e Palos Brito, Gabriel Teperino Cruz, Gabriel Paula Leite Müller, Guilherme Shimabuko Rocha e Silva, Marcos Guo Yan, Natasha dos Anjos Huang, Michelle de Almeida Paim de Andrade, and Hudson de Moraes Filho for having given me the best days of my life and support throughout the academic journey. You taught me the true meaning of friendship and I will carry our shared memories wherever I go.
Last but not least, I'm truly thankful for everyone else with whom I crossed path directly or indirectly. Special thanks to all professors, because nothing is possible without them.

Daniel Akira Ando

ABSTRACT

Direction of arrival (DoA) estimation is an important field of study, being required in civilian and military applications such as in wireless communications, search and rescue, law enforcement, sonar, and seismology. For all these applications, it is necessary to know the angle of arriving of an impinging radio signal on a receiver for further processing. Since the number of accidents and incidents involving unmanned aerial vehicles (UAVs) have increased in the past years, a probable application and also motivation for this study is the localizing of intruding UAVs.

Previous works on DoA estimation via received signal strength (RSS) value used platonic solid geometry associated with the multiple signal classification (MUSIC) algorithm. A DoA estimation algorithm with less computational complexity than the MUSIC algorithm is hereby presented, in which the differences of the RSS values measured between each directional antenna on the array is compared with the differences between their directivity gain pattern in order to estimate the direction of arrival of an incoming NTSC signal, which are typically used in UAVs. Different from the traditional phase-based DoA estimation techniques, which rely on, among others, the phase difference of the incoming signals, and thus need a previous time-consuming calibration process between the antennas on the array, the proposed RSS-based algorithm has a straightforward plug-and-play use, making it a simpler solution for applications such as the DoA estimation of UAVs.

After simulating the proposed technique and verifying its efficiency, the best angular spacing between the antennas on the array is computed. Then, field experiments were held with off-the-shelf and low-cost equipment, for instance, the AD-FMCOMMS5-EBZ daughter board containing the AD9361 receiver, video camera, NTSC transmitter and Yagi-Uda antennas. Experiments that accurately detect the direction of arrival of signals emitted from an intruder UAV is described.

RESUMO

Estimação da direção de chegada (do inglês: DoA) é um importante campo de estudo, sendo requerido em aplicações civis e militares como comunicações sem fio, busca e resgate, execução de leis, sonar e sismologia. Para todas essas aplicações, é necessário saber o ângulo de chegada de um sinal de rádio impingindo em um receptor para pós-processamento. Como o número de acidentes e incidentes envolvendo veículos aéreos não tripulados (VANTs) aumentou nos últimos anos, uma possível aplicação e também motivação para o presente estudo é a localização de VANTs invasores.

Trabalhos anteriores sobre a estimação do ângulo de chegada a partir da potência do sinal recebido (do inglês: RSS) fez uso de uma geometria sólida platônica associada com o algoritmo MUSIC (do inglês: Multiple Signal Classification). Um algoritmo para a estimação da direção de chegada com menor complexidade computacional que o MUSIC é apresentado neste trabalho,

no qual as diferenças das potências dos sinais recebidos em cada antena direcional do arranjo são comparadas com as diferenças dos padrões de ganho de diretividade de cada antena para a estimação do DoA de um sinal NTSC, tipicamente usado em VANTs. Diferente das técnicas tradicionais de estimação DoA baseadas na fase, as quais dependem, por exemplo, da diferença de fase dos sinais recebidos e, portanto, necessitam de uma extensa calibração prévia entre as antenas do arranjo, o proposto algoritmo baseado em RSS possui um uso mais direto e plug-and-play, tornando-o uma solução mais simples para aplicações como a estimação do DoA de VANTs.

Após as simulações da técnica proposta e da verificação de sua eficiência, o melhor espaçamento angular entre as antenas do arranjo é computado. Em seguida, experimentos em campo foram feitos com equipamentos de baixo custo, como, por exemplo, a placa controladora AD-FMCOMMS5-EBZ que contém o receptor AD9361, vídeo-câmera, transmissor NTSC e antenas Yagi-Uda. São descritos experimentos que precisamente detectam a direção de chegada de sinais emitidos de um VANT invasor.

TABLE OF CONTENTS

FIGURES LIST

TABLES LIST

Chapter 1

Introduction

1.1 Motivation

Recently, unmanned aerial vehicles (UAVs) have become a widely available product for the general consumer. In 2016, around 2 millions UAVs were sold for a variety of commercial and military applications [1]. The number of accidents and incidents involving them also increased in recent years [2], resulting in economical losses ranging from millions of dollars. Therefore, the development of a cost-efficient drone detecting system becomes necessary. A possible application of the direction of arrival (DoA) estimation technique proposed in this work is the detection and localization of intruding UAVs.

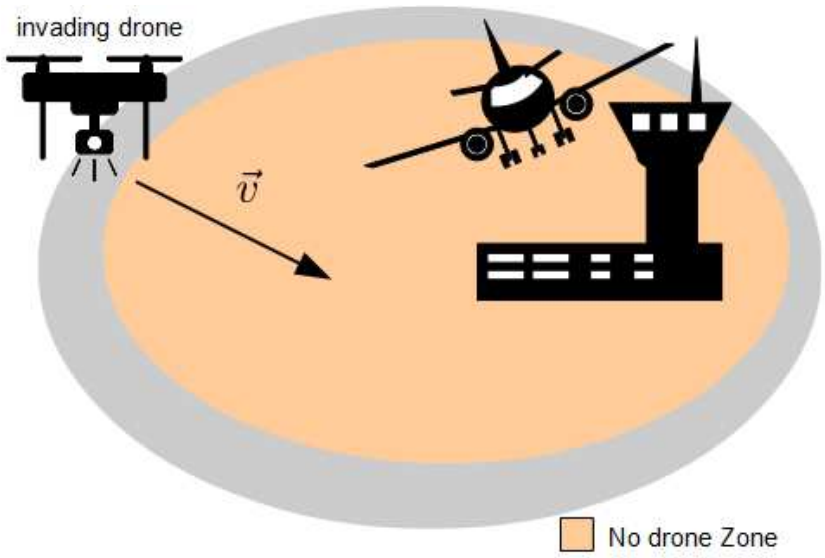

Figure 1.1: Drone invading an airport.

1.2 Objective

The aim of this work is to simulate the proposed technique of received signal strength based direction of arrival estimation with directional antennas in order to verify its validity, efficiency, and efficacy concerning the localization of unmanned aerial vehicles. We also propose to obtain the optimum angular spacing between the directional antennas on the array. This is useful to the design of an antenna array necessary for the motivation mentioned in Section 1.1 and to the fabrication of an optimum array arrangement capable of estimating the direction of arrival of a transmitting source with minimal estimation error. Lastly, our objective is to verify the performance of the proposed technique with field experiments by using low-cost off-the-shelf equipment.

1.3 Smart Antennas

Smart antenna systems consist of multiple antenna elements at the transmitting and/or receiving side of the communication link, whose signals are processed adaptively in order to exploit the spatial dimension of the mobile radio channel. Such spatial processing can increase the capacity of the wireless network by improving link quality through the mitigation of a number of impairments of mobile communications, such as multipath fading and co-channel interference, and by increasing the data rate through the simultaneous transmission of multiple streams by different antennas [3]. Some of the benefits of smart antennas can be summarized as follows [3]:

- Increased range/coverage;
- Lower power requirements and/or cost reduction;
- Improved link quality/reliability;
- Increased spectral efficiency.

An example of a smart antenna array with directional antennas is depicted in Figure 1.2.

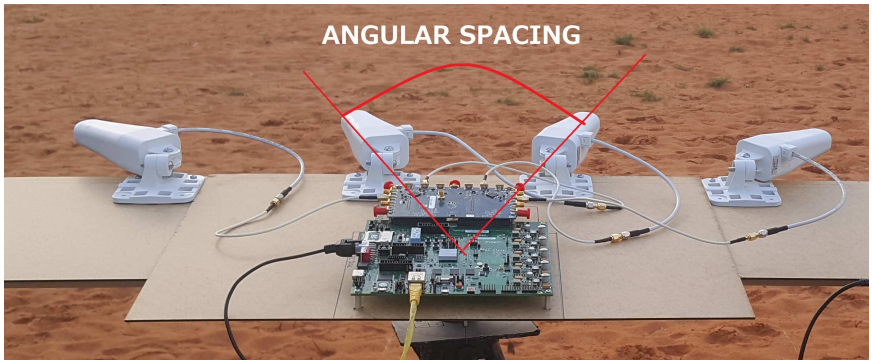

Figure 1.2: Smart antenna system with uniform array of directional Yugi-Uda antennas. The distance between two consecutive antennas is 20cm and they are angularly spaced at 40°.

The advantages mentioned earlier are due to the antenna array and the performance of digital signal processing (DSP) techniques used in the system. Examples of DSP techniques that play an important role in smart antenna systems are the direction of arrival (DoA) algorithms. They ensure that the array is able to estimate the direction of the incoming signal and use this information for further decision-making, such as pointing the array beam towards the estimated direction with the aid of adaptive beamforming in the case of wireless communication systems. In the present work, the estimation of the direction of arrival of the signal coming from an intruding UAV will be important to localize its position relative to the position of the array.

Some of the recent works on smart antennas are now presented. The authors in [4] present a method for signal adaptive sector selection, and develop two different alternatives for sector discretization. Also, they develop two novel methods for nonlinear interpolation based on nonlinear regression. One is derived from a nonlinear and nonparametric regression method called Multivariate Adaptive Regression Splines (MARS), the other approach extends the concepts of General Regression Neural Networks (GRNNs). Since arrays that have a Vandermonde or a left centro-hermitian response are very hard to achieve in real sensor array implementations, a mapping between the true and desired virtual array response can be created, and the received data can then be interpolated into this virtual array. The array is divided into multiple regions to be interpolated and there regions are discretized using a dense uniform grid. For each of these regions, a separate DoA estimation is performed.

In [5], the authors propose a framework composed of a bank of frequency invariant beamformers (FIB) and an adaptive parallel factor analysis (PARAFAC) decomposition. Beamforming is an array processing tool that provides spatial separation of multiple sources sharing the same spectrum band. It is a key technology to extract a signal of interest (SOI) and mitigate interfering signals.

In [6], tensor based techniques for antenna array based third generation GPS receivers are proposed. The authors conclude that the tensor based approaches, namely, Canonical Polyadic Decomposition - Generalized Eigenvalue Decomposition (CPD-GEVD) and Higher Order Singular Value Decomposition (HOSVD) combined with the L1C signaling and TMBOC modulation considerably outperform the state-of-the-art solutions and, thus, the incorporation of antenna array in the third generation GPS receivers and the inclusion of tensor based approaches are crucial to achieve accurate time-delay estimated in the presence of multipath components.

A high resolution framework with multipath mitigation for detecting and locating a signal emitter randomly positioned within a region of interest is proposed in [7]. The proposed framework detects the signal of interest and provides the number of line-of-sight (LOS) plus non-line-of-sight (NLOS) components by applying model order selection schemes. Next the multipaths are mitigated by exploiting the signal structure and estimating the DoA of each component. Finally, the estimated DoAs are triangulated, thus providing the source position.

There are two types of antennas which can be used to compose an smart antenna array: omnidirectional antennas or directional antennas. Omnidirectional antennas are defined as antenna elements that have equal radiation along the azimuthal directions but varying radiation along the elevation direction. Directional antenna elements are defined as the elements that are able to

concentrate the power primarily in certain directions or angular regions. The advantages of this type of elements compared with the omnidirectional ones are the ability to focus their power to the desired direction and to suppress noise signals simultaneously[8].

1.3.1 Yagi-Uda Antennas

The type of antenna used during this entire work is the Yagi-Uda antenna, which is a parasitic linear array of parallel dipoles. Parasitic arrays are array configurations where there is only one element directly connected to a transmitter and/or receiver while the other elements (called parasitic elements) receive their excitation by near-field electro-magnetic coupling from the driven element. By doing so higher gain can be achieved. The typical configuration of Yagi-Uda antennas consist of three elements: the driver, reflector and director elements as shown in Figure 1.3.

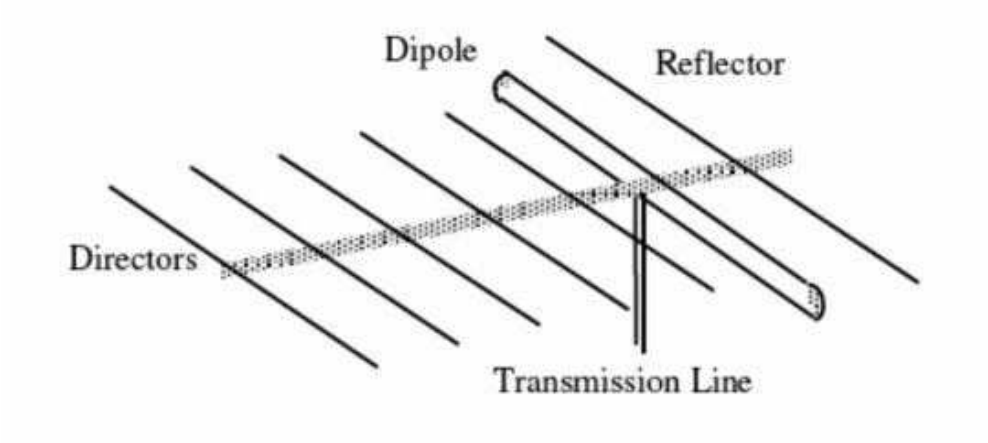

Figure 1.3: Yagi-uda antenna configuration.

1.4 Direction of Arrival Estimation

Direction of Arrival (DoA) estimation (or direction finding, angle of arrival estimation) is essentially the estimation of the direction of arrival of electromagnetic signals or acoustic waves impinging on a sensor or antenna array. As it can be seen in Figure 1.4 the signal is impinging on a uniform linear array (ULA) with an angle θ_0. DoA estimation algorithms are used to estimate the value of θ. Some of the applications of this estimation can be seen in telecommunications, wireless emergency calls location, search and rescue, radar, sonar, seismology [9].

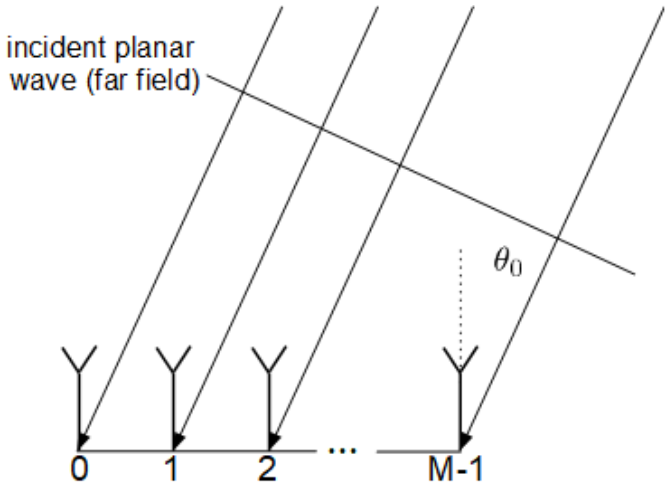

Figure 1.4: Uniformly spaced linear array containing M omnidirectional antenna elements. The incident signal wave coming from a source located in the far-field of the antennas is considered to be a plane wavefront.

Direction of arrival estimation algorithms are normally incorporated to smart antennas to develop systems that provide accurate location information for wireless services. Together, smart antenna and DoA algorithms can be used to enhance the mobile communications coverage, to increase system capacity and to spatially separate signals [9].

In general, the direction of arrival estimation algorithms can be classified into:

- Beamforming techniques;
- Maximum likelihood techniques;
- Subspace-based techniques.

The basic idea behind beamforming techniques is to "steer"the array in one direction at a time and measure the output power. When the "steered"direction coincides with a DoA of a signal, the maximum output power will be observed. The development of the DoA estimation schemes is essentially the design of an appropriate form of output power that will be strongly related to the DoA. Some examples of beamforming techniques are Capon and Linear Prediction [10].

Maximum likelihood (ML) techniques were some of the first techniques investigated for DoA estimation. Given a received data sequence $\mathbf{x}(t_n)$, it is desired to reconstruct the components of the data due only to the desired signals. The parameter values for which the reconstruction approximates the received data with maximal accuracy are taken to be the DoA [11].

Subspace-based algorithms are high resolution techniques which exploit the eigen-structure of the input data or covariance matrix. The Multiple Signal Classification (MUSIC) algorithm was one of the first to exploit the structure of the input data matrix for the case of arrays of arbitrary geometry. The Estimation of Signal Parameters via Rotational Invariance Techniques (ESPRIT)

algorithm is a subspace-based technique applicable to arrays, such as the uniform linear array (ULA), that possess a displacement invariant structure [12].

The above mentioned techniques are mainly classified as phase-based direction of arrival estimation algorithms. When simplicity is required, that is, when no special hardware is required, signal strength or amplitude based algorithms are also preferred for DoA estimation [13].

1.4.1 RSS-based Direction of Arrival Estimation

Different from phase-based direction of arrival estimation techniques, that use the difference in the phase of the incoming signals at the antennas on the array to estimate θ, received signal strength (RSS) based techniques use the signal strength or amplitude information to estimate it. This is possible because of the gain pattern of antennas, that are the angular description of their directivity gain. In other words, this pattern provides us the information of how the directivity gain of an antenna angularly changes, and direction of arrival can be estimated through the knowledge of this information.

Some of the works that use RSS-based DoA estimation are briefly presented. In [14], the author shows how an algorithm, which employs received signal strength values in order to estimate the DoA of impinging signals in wireless sensor network (WSN) nodes equipped with electronically steerable parasitic array radiator (ESPAR) antennas, can be improved by applying an interpolation algorithm to radiation patterns recorded in the calibration phase of the DoA estimation process. The DoA estimation method used in this work is called Power Pattern Cross-Correlation (PPCC) algorithm [15], in which only the recorded RSS values at the ESPAR antenna's output is used for the estimation. This algorithm relies on cross-correlation coefficient that is calculated between the antenna output recorded for different main beam directions and previously measured antenna's radiation patterns. The author concludes that the proposed method made it possible to estimate the direction of the signal impinging on the antenna with similar RMS errors and precisions while only having 30 calibration points per single radiation pattern, instead of 360 used when no interpolation of radiation pattern is applied.

The authors in [16] propose a novel localization scheme, called Angle of Arrival Localization with RSSI Differences (ALRD) to estimate angle-of-arrival (AoA) by comparing the RSSI values of beacon signals received from two perpendicular-oriented directional antennas installed at the same place. The RSSI values received from a directional antenna are fitted into a parabola function of AoA between 0° and 90° by quadratic regression analysis and the difference between the signals RSSI values of the two perpendicular-oriented directional antennas are fitted into a linear function of AoA between 0° and 90° by linear regression analysis. This ALRD algorithm is based on the RSSI-fitting functions. After indoor experiments they concluded that the proposed algorithm embedded in a sensor node can estimate its location within 0.1 second with an average localization error of 124 cm.

In the work done in [13], the authors establish the theoretical framework of received signal strength (RSS) based direction finding with an array of directional antennas with normal density

distribution in magnitude. The angle of arrival and the distance between the array and the emitter are jointly estimated by means of maximum likelihood estimation (MLE). They calculate the Cramer Rao Lower Bound (CRLB) for the joint estimation of angle of arrivel and incident signal power, and the major component of the CRLB calculations is to model the radiation patterns of directional antennas as von Mises distributions (i.e. circular version of normal distribution). They conclude that the CRLB is not a function of angle of arrival. That means that all angles have the same level of error. It was also concluded that the CRLB is inversely proportional do the directivity of the antennas. By means of Monte Carlo simulations, they show that the plots of MLE and CRLB overlap each other and the estimation error of these RSS-based directional antenna systems are acceptable.

A proof-of-concept device and method to estimate the DoA of a radio signal by a receiver that is suitable for wireless sensor networks (WSN) applications is presented in [17]. The device estimates the DoA by identifying the peak of received signal strength indicator measurements using an actuated parabolic reflector. When the reflector is aligned in such a way that the incoming signal is focused at the receiver antenna, a high RSSI value is observed, while at other orientations of the reflector a lower RSSI is observed. It is concluded in this work that it is possible to measure DoA from RSSI with equally good performance both indoor and outdoor by using an actuated parabolic reflector as long as there are no moving objects in the vicinity of the transceivers.

In [18], a single-antenna power measurements based direction finding technique that estimates the direction of arrival from a vector of power measurements is proposed. This technique exploits the diversity in the antenna radiation pattern that is captured through the received power calculated when the antenna is pointing at different directions. From a vector of power measurements, the mentioned approach first utilizes a linear transformation of the power vector into a vector of spectral observations. The DOAs are then estimated as the solution to the spectral analysis. Through simulations and experimental results, the feasibility of the proposed single power measurements based direction finding is demonstrated.

Chapter 2

Proposed RSS-based DoA Estimation

2.1 Introduction

In this chapter, the proposed received signal strength (RSS) based direction of arrival estimation technique is presented. After describing the state-of-the-art and the proposed technique, the algorithm for this RSS-based DoA estimation will be validated through simulation. The main purpose of the simulation, besides the verification of the validity of the proposed algorithm, is to find the optimum angular spacing ϕ_{opt} between the antennas of the array. This chapter is divided in the following sections: In Section 2.2 the data model of this proposed technique is presented. In Section 2.3 the state-of-the-art is described. In Section 2.4 the mathematical description of this algorithm is presented. In Section 2.5 the results obtained from the simulation are shown, and the best angular spacing is calculated.

2.2 Data Model

This section presents the data model necessary for the subsequent derivation of the proposed direction of arrival estimation technique. First, the antenna array arrangement for the case of M antennas will be presented. Then, the vector $\mathbf{p}_{\text{rx}}(\theta)$ is defined, which contains the RSS values measured in each antenna of the array. At last, the M-antenna array directivity gain pattern vector $\mathbf{g}_{\text{array}}(\theta)$ is defined.

The M-directional-antenna array arrangement with the associated reference axes is shown in Figure 2.1. The angular spacing between each antenna is given by ϕ, the perturbation in this spacing is given by σ_ϕ, and the transmitter direction of arrival is given by θ.

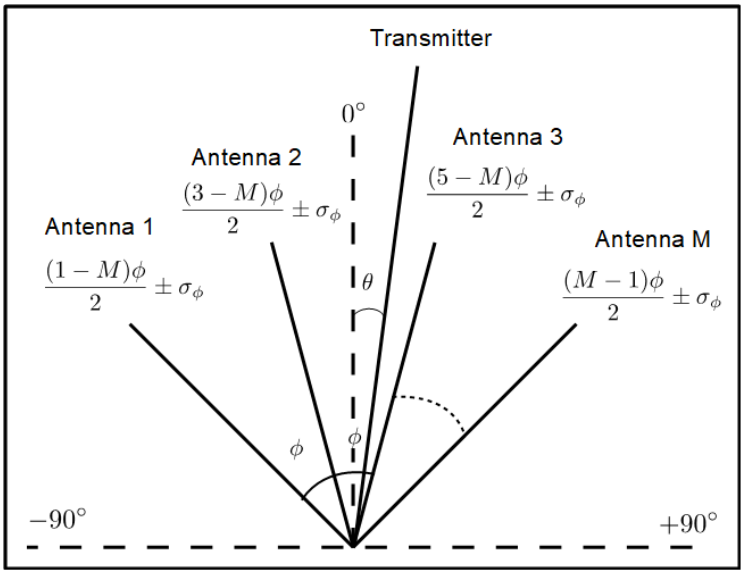

Figure 2.1: Graphical representation of the directional antenna array and transmitter position.

For the calculation of the direction of arrival estimation, the received signal strength at each antenna of the array is used. According to the Friis's Transmission Equation [19] the RSS $P_{\text{rx}}(\theta)$ at one directional antenna with gain pattern $g(\theta)$ is:

$$P_{\text{rx}}(\theta) = P_{\text{tx}} + G_{\text{tx}} + g(\theta) + 20\log_{10}\left(\frac{c}{4\pi R f}\right); \tag{2.1}$$

where P_{tx} and G_{tx} are the transmission power and gain, respectively, c is the speed of light, R is the distance between transmitter and receiver, and f is the transmission frequency. Thus, the received signal strength vector $\mathbf{p}_{\text{rx}}(\theta)$ is computed as follows:

$$\mathbf{p}_{\text{rx}}(\theta) = \begin{bmatrix} P_{\text{rx,1}}(\theta) & \cdots & P_{\text{rx,M}}(\theta) \end{bmatrix}^{\text{T}} + \mathbf{n}, \tag{2.2}$$

where $P_{\text{rx},i}(\theta)$, $i = 1, \cdots, M$ is the RSS at antenna i and $\mathbf{n} = [n_1 \quad \cdots \quad n_M]^{\text{T}}$ is a vector containing random variables with Gaussian distribution $\mathcal{N}(0, \sigma^2_{\text{rss}})$.

The M-antenna array directivity gain pattern is obtained as follows:

$$\mathbf{g}_{\text{array}}(\theta) = \begin{bmatrix} g(\theta+\phi_1) & \cdots & g(\theta+\phi_{\text{M}}) \end{bmatrix}, \tag{2.3}$$

where ϕ_i, $i = 1, ..., M$, is the angular shift of the location of the antenna i. In the case of equally angular spaced antennas, $\phi_i = (i-1)\phi - \frac{(M-1)\phi}{2}$, ϕ being the angular spacing between the antennas. If an off-the-shelf directional antenna is used, it is also important to notice that there is a positioning error σ_ϕ that alters the true positioning value ϕ_i. During the simulation the effect of this perturbation on the DoA estimation will be verified.

2.3 State-of-the-Art

The work done in [20] presents the theoretical analysis and the experimental evaluation of a new switched beam antenna designed to operate at 2.45 GHz. The antenna enables direction of

arrival estimation using six directional planar elements arranged in a platonic solid geometry. First, for a target positioning using DoA information, their estimation is based on the RSS measured on each antenna element. To remove the dependence of the signal power incident at the antenna array, the differences in received power between any two faces of their array is computed. The reason why this is done lies in the Friis's Transmission Equation [19]. Consider an omni-directional transmitter located in the far-field from both receivers. Thus, the term $P_{\text{tx}} + G_{\text{tx}} + 20\log_{10}\left(\frac{c}{4\pi Rf}\right)$ from Equation (2.1) is the same for the receivers.

$$P_{\text{rx},i}(\theta) = P_{\text{tx}} + G_{\text{tx}} + g(\theta + \phi_i) + 20\log_{10}\left(\frac{c}{4\pi Rf}\right), \tag{2.4}$$

$$P_{\text{rx},j}(\theta) = P_{\text{tx}} + G_{\text{tx}} + g(\theta + \phi_j) + 20\log_{10}\left(\frac{c}{4\pi Rf}\right), \tag{2.5}$$

By subtracting Equations (2.4) and (2.5), only the dependency on the antenna gains remains:

$$P_{\text{rx},i}(\theta) - P_{\text{rx},j}(\theta) = g(\theta + \phi_i) - g(\theta + \phi_j). \tag{2.6}$$

Further on, the DoA of the target's messages are estimated by using the power differences with the multiple signal classification (MUSIC) algorithm [20]. Their measurement results reveal that their system is able to estimate the DoA with a good accuracy for the azimuth angle, while the inclination angle showed an almost constant bias.

2.4 Proposed Technique

In this section a technique to estimate the direction of arrival of one transmitting source by measuring the received signal strength in each antenna of the array, computing the differences of one RSS with another, and comparing them with the differences of the directivity gain pattern of the antennas is proposed. The result of subtracting the received powers at two different antennas is the difference of their directivity gains. The DoA is then estimated by comparing these RSS differences with the array gain pattern.

First, we define the matrix $\mathbf{P}(\theta) \in \mathbb{R}^{M\times M}$, whose elements $[\mathbf{P}(\theta)]_{i,j}$ are:

$$[\mathbf{P}(\theta)]_{i,j} = \begin{cases} P_{\text{rx},i}(\theta) - P_{\text{rx},j}(\theta), & \text{if } i < j, \\ \bar{\delta}_1(i,j)P_{\text{rx},1}(\theta) + \cdots + \bar{\delta}_M(i,j)P_{\text{rx},M}(\theta), & \text{if } i > j, \\ 0, & \text{otherwise,} \end{cases} \tag{2.7}$$

where M is an even number, $\bar{\delta}_k(i,j) = (2\delta(i-k)-1)(2\delta(j-k)-1)$ and $\delta(x)$ is the unitary impulse function returning 1 at $x = 0$ and 0 elsewhere. In the first line in Equation (2.7), which is the difference between the RSS in two different antennas, the state-of-the-art is referred, and in the second line the M-tuple RSS difference between the M antennas is referred. The function $\bar{\delta}_k(i,j)$ indicates the position of the negative sign according to the combination $\binom{M}{\frac{M}{2}}$.

Then, the difference vector $\mathbf{p}(\theta)$ is computed:

$$\mathbf{p}(\theta) = \text{vec}(\mathbf{P}(\theta)), \tag{2.8}$$

where vec(.) is an operator that creates a vector out of a matrix. However, in this proposed technique, only the nonzero values of the matrix $\mathbf{P}(\theta)$ are taken to compute the difference vector $\mathbf{p}(\theta)$.

Then, the spatial power response $P(\theta)$ is calculated, which will carry the information on where the DoA is by comparing the RSS with the array gain pattern.

$$P(\theta) = \frac{1}{||\mathbf{g}(\theta) - \mathbf{p}(\theta)||_2^2}. \tag{2.9}$$

The vector $\mathbf{g}(\theta)$ contains the differences between the known antenna patterns $g(\theta)$, defined in the same way as the difference vector $\mathbf{p}(\theta)$, by firstly computing a matrix $\mathbf{G}(\theta) \in \mathbb{R}^{M \times M}$ and then vectorizing it by only taking the nonzero values:

$$[\mathbf{G}(\theta)]_{i,j} = \begin{cases} g_i(\theta) - g_j(\theta), & \text{if } i < j, \\ \bar{\delta}_1(i,j)g_1(\theta) + \cdots + \bar{\delta}_M(i,j)g_M(\theta), & \text{if } i > j \\ 0, & \text{otherwise,} \end{cases} \tag{2.10}$$

$$\mathbf{g}(\theta) = \text{vec}(\mathbf{G}(\theta)), \tag{2.11}$$

where $g_k(\theta) = g(\theta + \phi_k)$, $k = 1, ..., M$ for simplicity.

Subsequently, the maximum point of $P(\theta)$ will give the estimated DoA $\hat{\theta}$, which can be estimated via maximization of Equation 2.9:

$$\hat{\theta} = \underset{\theta}{\text{argmax}}(P(\theta)). \tag{2.12}$$

2.5 Simulations

In this section, simulations are carried in order to validate the algorithms shown in Sections 2.3 and 2.4. Also, the best antenna spacing ϕ_{opt} is found by means of Monte Carlo trials. Initially, the signal power received in each antenna $P_{\text{tx},i}(\theta)$, $i = 1, ..., M$, for antenna i, is simulated by using the Friis's Transmission Equation [19]. Different values of $P_{\text{tx},i}(\theta)$ are obtained by varying the transmitter position θ, the angular spacing ϕ between the antennas, and the perturbation σ_ϕ in the angular spacing. To simplify the simulation the noise $\mathbf{n}$ (see Equation 2.2) will not be considered. Subsequently, both vectors $\mathbf{p}(\theta)$ and $\mathbf{g}(\theta)$ defined in section 2.4 are computed in order to estimate the direction of arrival. Finally the error is computed for every direction of arrival estimation. By plotting the errors, we can analyze the performance of this technique and calculate the best angular spacing between the antennas.

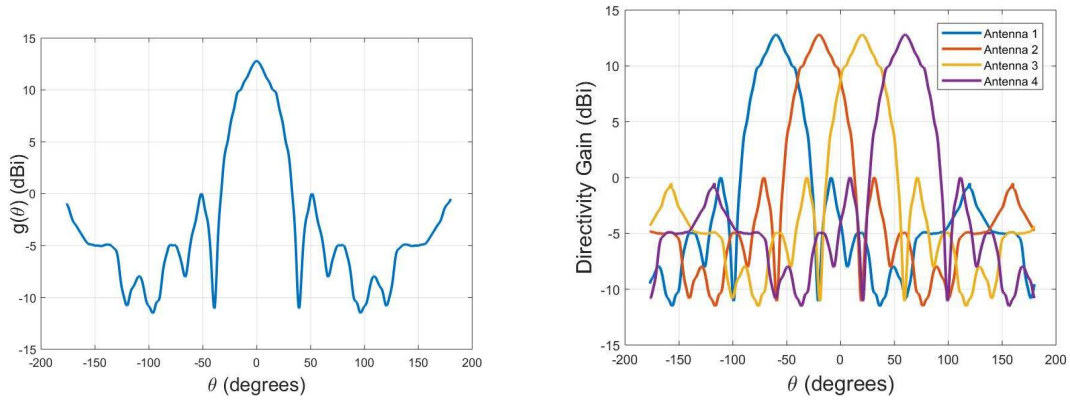

(a) (b)

Figure 2.2: (a) Directivity gain pattern provided by the manufacturer of the directional antenna used during the experiments and (b) 4-antenna array directivity gain pattern with an angular spacing $\phi = 40°$.

The directivity gain pattern of one of the directional antennas used during the experiments (Section 3) was supplied by the manufacturer and it is simulated as shown in Figure 2.2(a). Since four directional antennas will be used for the experiments, the array gain pattern is depicted in Figure 2.2(b).

The NTSC transmitter that is used for the field experiment detailed in Chapter 3 has an output power of 200mW at a frequency of 5.685GHz. After some calculation, it is found that the transmitter should be at a distance at least 40m apart from the receiving array in order to diminish the different angular incidence of the impinging plane wave on each antenna. Thus, with these parameters (P_{tx}, f, R) the received power at one antenna can be simulated and is shown in Figure 2.3.

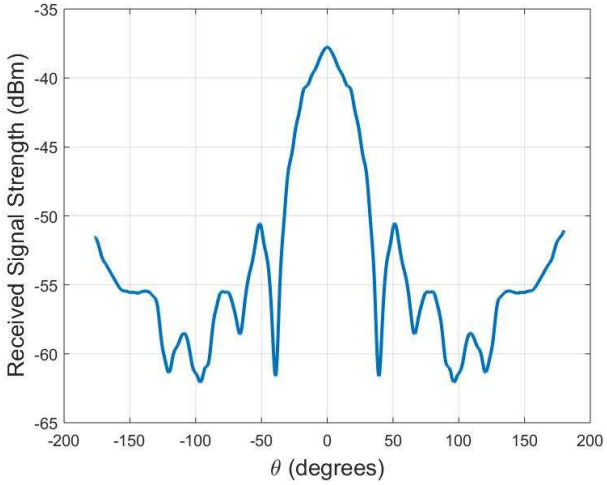

Figure 2.3: Simulated received signal strength at one antenna for $P_{\text{tx}} = 200\text{mW}$, $f = 5.685\text{GHz}$, and $R = 40\text{m}$.

Now the values of received signal strength in each one of the four directional antennas on the array can be simulated by taking into consideration the perturbation σ_ϕ and the vectors $\mathbf{p}(\theta)$ and $\mathbf{g}(\theta)$ are computed. To illustrate how the technique works, consider a source transmitting at $\theta = 0°$. The RSS vector is $\mathbf{p}_{\text{rx}}(\theta = 0°) = [-59.3733 \quad -47.6079 \quad -47.1418 \quad -59.4613]^{\text{T}}$. Then the difference vector $\mathbf{p}(\theta)$ is calculated and $\mathbf{p}(\theta = 0°) = [-11.7654 \quad -12.2315 \quad 0.0880 \quad -0.4661 \quad 11.8533 \quad 12.3194]^{\text{T}}$ is obtained. The algorithm then compares the vector $\mathbf{p}(\theta)$ with the vector $\mathbf{g}(\theta)$ via Equation 2.9 in order to find the direction of arrival.

Table 2.1: Table containing values for vector $\mathbf{g}(\theta)$.

θ	$\mathbf{g}(\theta)^{\text{T}}$
$-90°$	[10.0413 11.5256 8.5000 1.4843 -1.5413 -3.0256]
$-60°$	[23.4318 17.7288 23.6000 -5.7031 0.1682 5.8712]
$-30°$	[-7.5381 3.8251 13.5000 11.3632 21.0381 9.6749]
$0°$	[-12.7393 -12.7393 0 0 12.7393 12.7393]
$+30°$	[-9.6749 -21.0381 -13.5000 -11.3632 -3.8251 7.5381]
$+60°$	[-5.8712 -0.1682 -23.6000 5.7031 -17.7288 -23.4318]
$+90°$	[3.0256 1.5413 -8.5000 -1.4843 -11.5256 -10.0413]

As it can be seen in Table 2.1, the vector $\mathbf{p}(\theta)$ is near the vector $\mathbf{g}(\theta)$ at $\theta = 0°$. This can be verified by plotting the spatial power response $P(\theta)$ as shown in Figure 2.4.

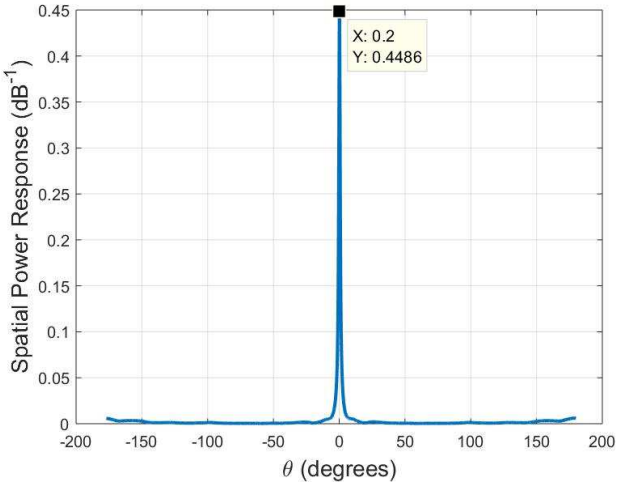

Figure 2.4: Spatial Power Response for $\theta = 0°$. The absolute error $|\theta - \hat{\theta}|$ is $0.2°$.

Other examples of the calculation of the spatial power response are shown in Figure 2.5.

Now the absolute error is computed for all values of θ between $-90°$ and $+90°$ and is shown in Figure 2.6. From this figure, it is noticeable that the absolute error in the direction of arrival estimation for $-90° \leq \theta \leq 90°$ is mostly below $8°$, which means that the proposed technique is suitable for the detection of UAVs with good efficiency.

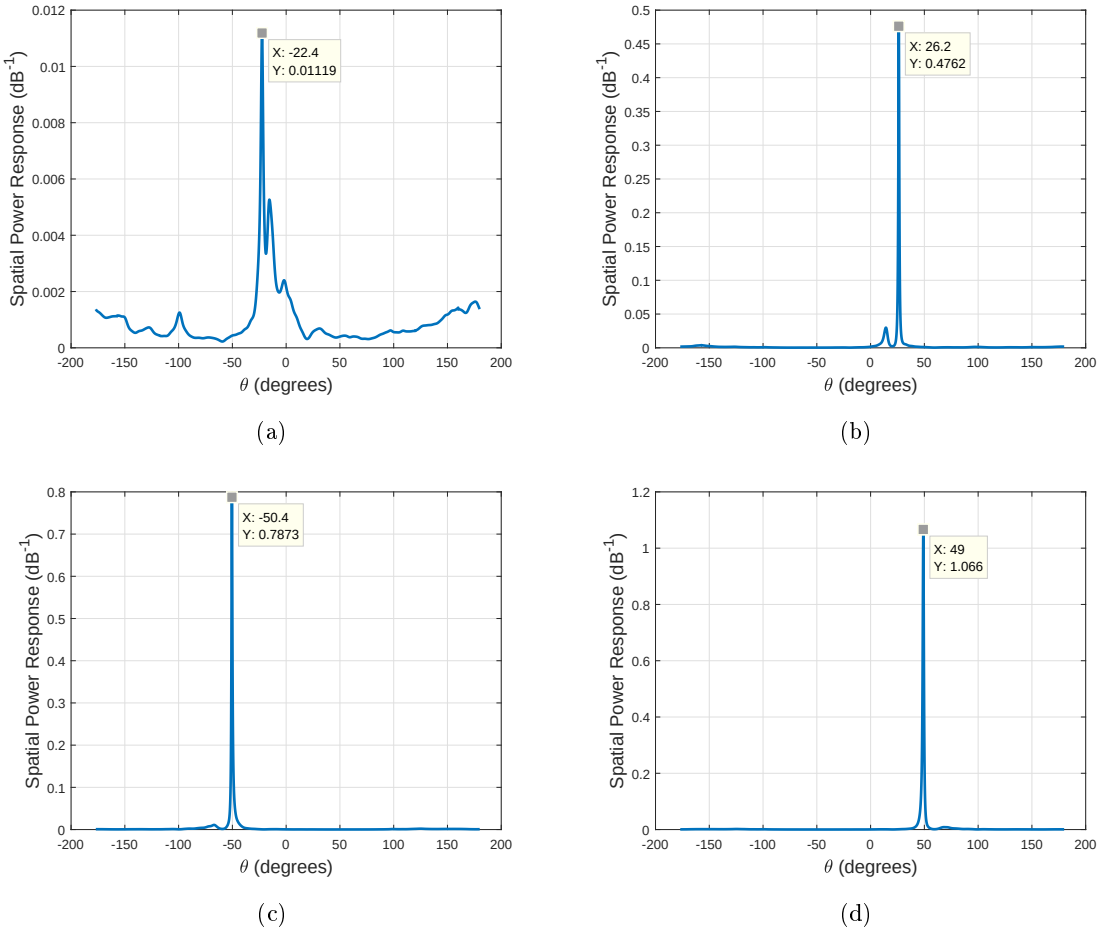

Figure 2.5: Spatial Power Response for the cases: (a) $\theta = -25°$ with $|\theta - \hat{\theta}| = 2.6°$. (b) $\theta = +25°$ with $|\theta - \hat{\theta}| = 1.2°$. (c) $\theta = -50°$ with $|\theta - \hat{\theta}| = 0.4°$. (d) $\theta = +50°$ with $|\theta - \hat{\theta}| = 1.0°$

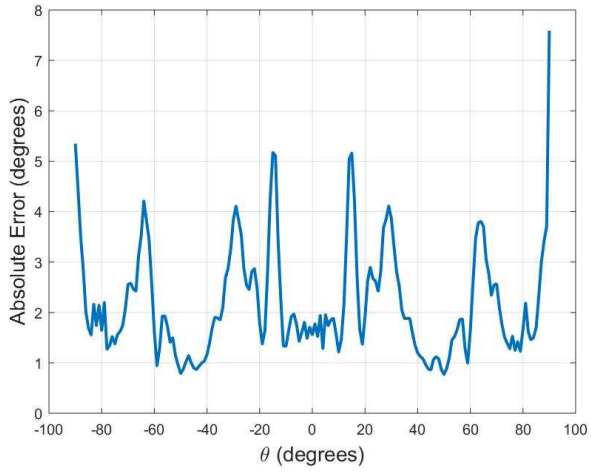

Figure 2.6: Absolute error computed for values of θ between $-90°$ and $+90°$.

As a next step, the perturbation σ_ϕ will be varied while fixing the angular spacing ϕ to verify

how the absolute estimation error responds. Since this perturbation is essentially due to the precision in the rotating of the antennas from one another, this part of the simulation is useful for us to understand how badly the system worsens for a lesser rotation precision. We notice by looking at Figure 2.7 that for a larger perturbation σ_ϕ, the estimation error also becomes larger for all angular spacing ϕ. However, the more we rotate the antennas away from each other, that is, the larger we make ϕ, the less absolute error we can achieve for a wider range of transmitter position θ. From this result, we can already foresee that a wider ϕ is wanted for a better direction of arrival estimation, but how wide? This will be confirmed later in this section.

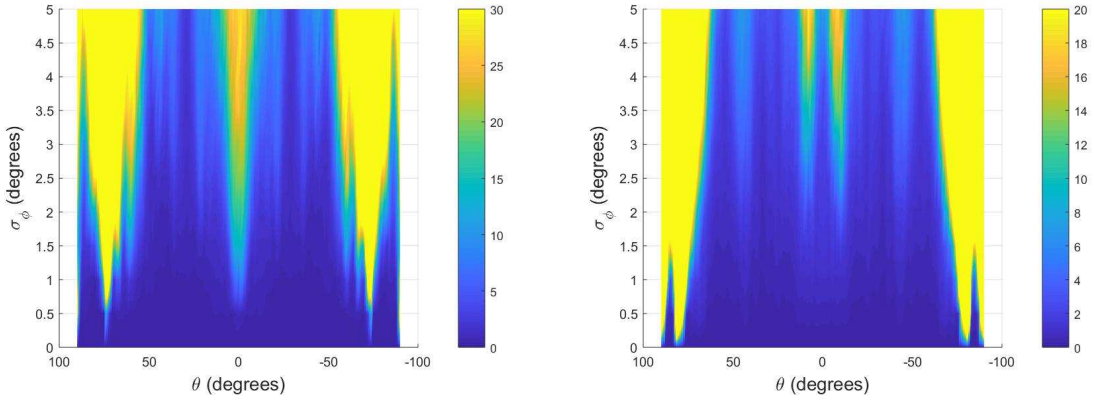

(a) $\phi = 20°$

(b) $\phi = 30°$

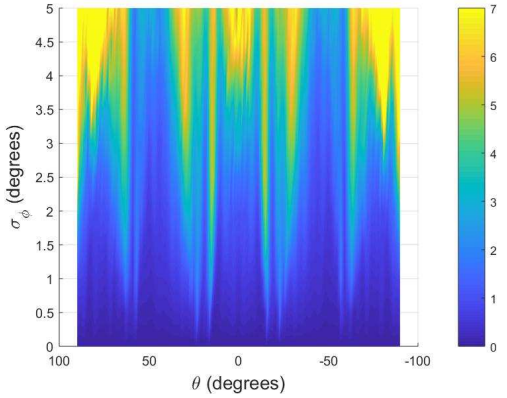

(c) $\phi = 40°$

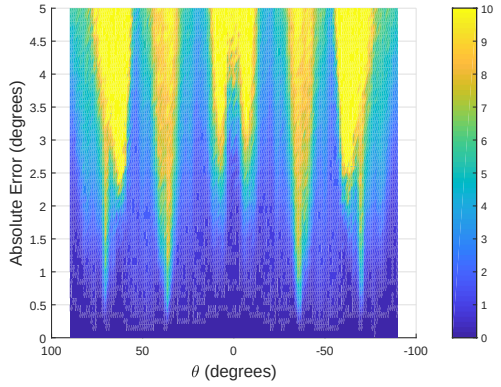

(d) $\phi = 60°$

Figure 2.7: Absolute error in degrees computed for varying values of σ_ϕ while fixing ϕ.

A value of 2.5° is chosen for the perturbation σ_ϕ which is roughly the achieved precision with the available equipment. In other words, after performing measurements with the protractor, we concluded that there is an average error of 2.5°. Thus, it is now possible to verify how the absolute estimation error variates as we variate the angular spacing ϕ.

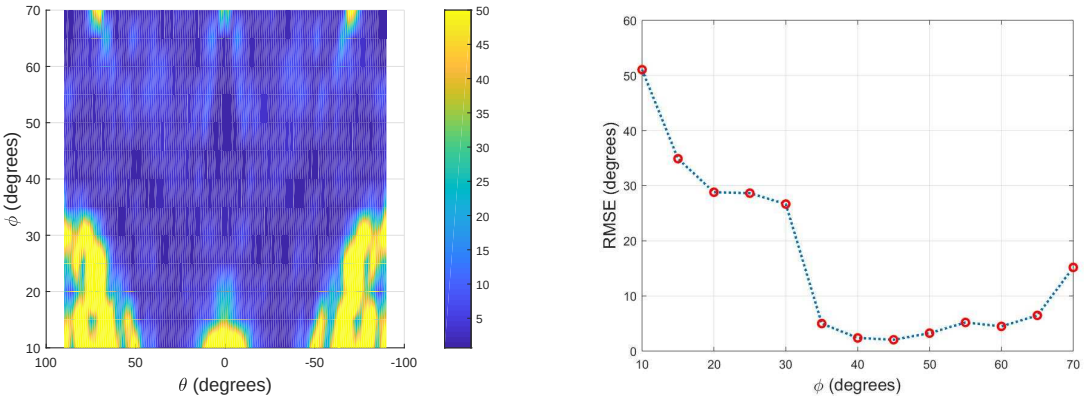

(a) Absolute error for a fixed σ_ϕ and varying ϕ

(b) Root-mean-square error

Figure 2.8: Best angular spacing ϕ_{opt}

As we can observe in Figure 2.8(b), values of $35° \leq \phi \leq 65°$ achieve a root-mean-square error less than $10°$. This is a desirable value for our purpose of localizing the azimuth of UAVs. Therefore, for the subsequent field experiments, a value of angular spacing ϕ inside this interval ought to be chosen.

Chapter 3

Experimental Results

3.1 Introduction

In this chapter, the field experiment necessary to validate the proposed RSS-based direction of arrival estimation technique and to show that this system works efficiently with relatively low-cost equipment and off-the-shelf directional antennas is presented. This chapter is divided as follows: In Section 3.2, the equipments used in the experiment and the methodology are detailed. In Section 3.3, the received signal strength indicator (RSSI) is defined and the conversion between RSSI and dBm for the case of the hardware in use is presented. Lastly, in Section 3.4 the results and further analysis of the field experiments are presented.

3.2 Experiment Description

3.2.1 Equipment

For this experiment, the following equipment were used:

- AD-FMCOMMS5-EBZ and AD9361;
- Xilinx Zynq-7000 SoC ZC706;
- YE572113 Yagi-Uda antennas;
- 5.8GHz 200mW NTSC Transmitter;
- Custom built 5.8GHz LHCP antenna;
- Video camera;

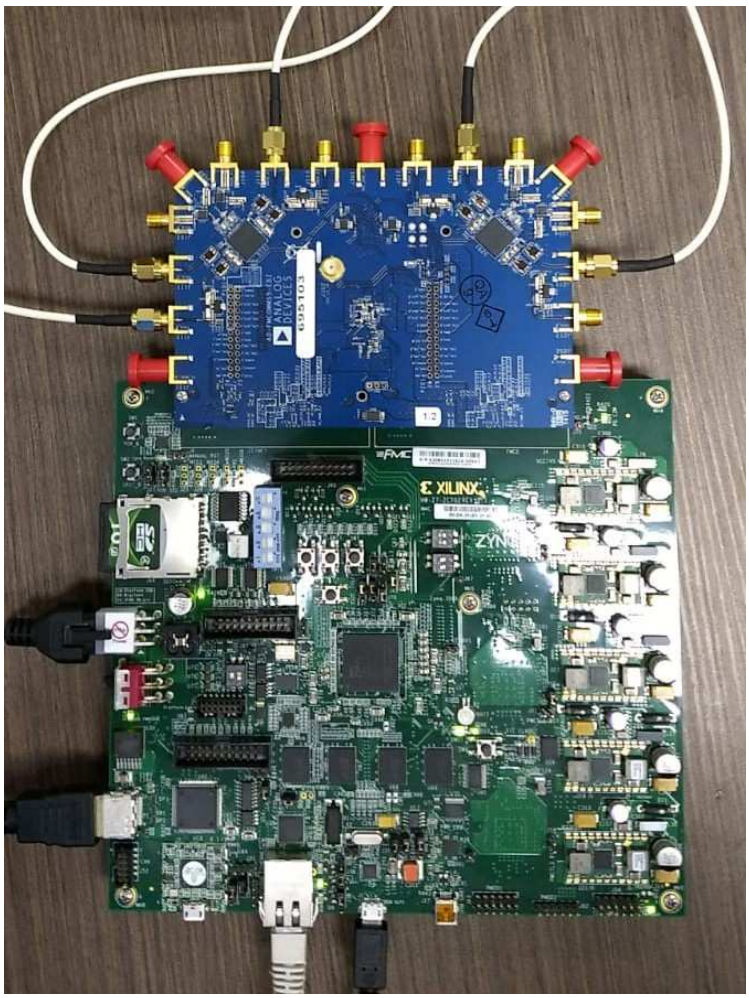

Figure 3.1: Xilinx Zynq-7000 SoC ZC706 carrier board (below) connected with the AD-FMCOMMS5-EBZ (above).

The AD9361 and the boards shown in Figure 3.1 are used for the RF reception of the NTSC signal emitted by, for example, an UAV. The AD9361 is an integrated RF transceiver with programmability and wideband capability for various transceiver applications. It combines an RF front-end with a mixed-signal baseband section and integrated frequency synthesizers, and operates in the 70MHz to 6GHz range. The AD-FMCOMMS5-EBZ board contains two AD9361s in a 4 x 4 RF configuration and possesses the features and capabilities of the chip. This board is attached to a carrier board for data acquisition containing a Xilinx Zynq-7000 SoC ZC706.

(a) Yagi-Uda antenna used in the experiment.

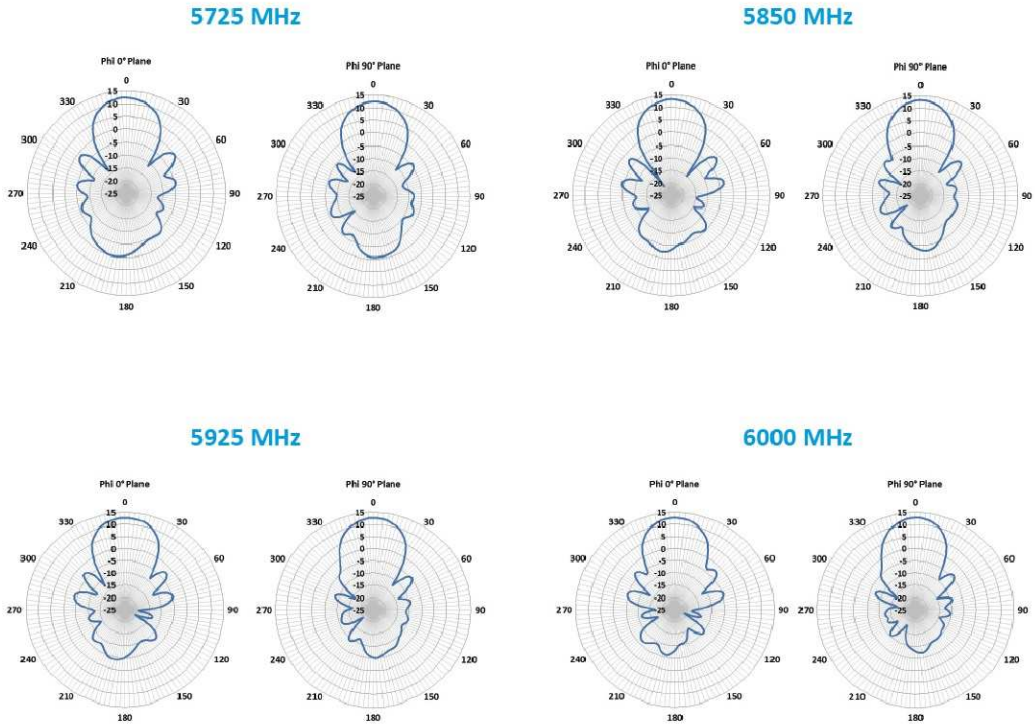

(b) Directional gain pattern of the Yagi-Uda antenna.

Figure 3.2: RF reception hardware.

Four of the Yagi-Uda antenna shown in Figure 3.2(a) were used during the field experiments and were connected in the AD-FMCOMMS5-EBZ board shown in Figure 3.1. In Table 3.1 their details and specifications are shown. It is a Laird YE572113 12.5dBi gain directional antenna that operates in the 5725-6000MHz band. It also contains an articulating arm mount which enables us to rotate the antennas in order to position them in the desired angular spacing ϕ. In Figure 3.2(b)

the directional gain pattern measured by the manufacturer is also shown.

Table 3.1: Specifications of the Yagi-Uda antennas

PARAMETER	SPECIFICATIONS		
Model	YE572113		
Frequency Bands, MHz	5725 - 5850	5850 - 5925	5925 - 6000
Peak Gain, dBi (Avg)	12.5	13.0	12.7
Peak Gain, (Max)	13.2	13.2	12.9
VSWR, Avg	1.4:1	1.2:1	1.4:1
VSWR, Max	1.8:1	1.5:1	2.0:1
Nominal Impedance	50 Ω		
Polarization	Vertical or Horizontal		
Azimuth 3dB Beamwidth	35°		
Elevation 3dB Beamwidth	35°		
Front-to-Back Ratio	15 dB		
Side Lobe	14 dB		
Max Power (Ambient 25°C)	25 Watts		
Antenna Dimension (L x W)	149.1 x 58.6 mm		
Weight w/ Bracket	0.16 kg		
Antenna Color	White		
Radome	ASA, UV Stable		
Wind Operational	160 km/h		
Wind Survival	220 km/h		
Operating Temperature	−30°C to +70°		
Storage Temperature	−40°C to +80°		
Ingression Protection	IP67		
Material Substance Compliance	RoHS		

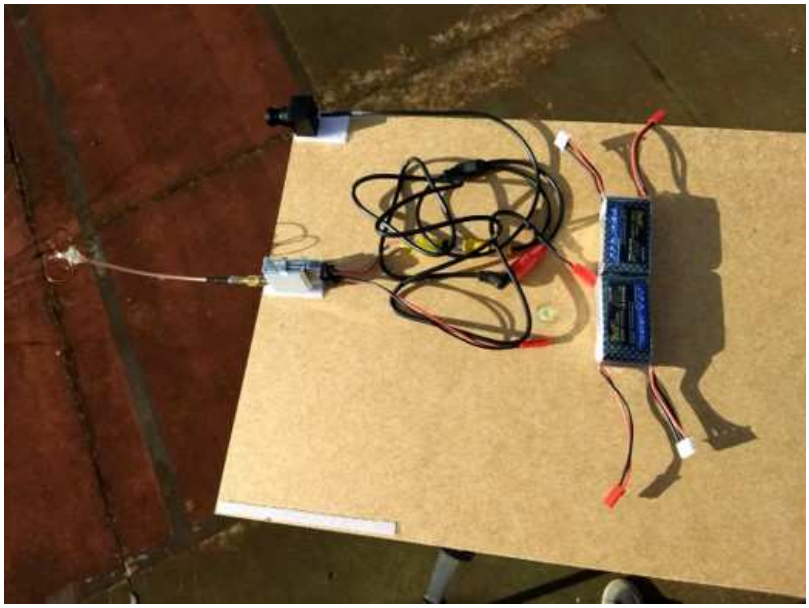

Figure 3.3: Transmission equipment used in the field experiments.

In Figure 3.3 it is shown the video camera, the 5.8GHz 200mW NTSC transmitter, and the custom built 5.8GHz LHCP antenna used in the field experiments. Considering the non-planar flying movement of a drone and the fact that LHCP antennas are commonly used, the LHCP antenna was chosen as the transmitter antenna. Both the video camera and NTSC transmitter were acquired in the same UAV set.

3.2.2 Methodology

(a) (b)

Figure 3.4: Environment where the experiment was held.

The location where the experiment took place and where both transmitter and receiver were is shown in Figure 3.4. A distance of 20cm was calculated to place the antennas separated from one another on top of a wooden base. For the experiments, we positioned the antennas $\phi = 40°$ apart from each other. Both transmitter and receivers were mounted on a tripod 115cm above the

ground and were placed 38m apart.

The transmitter sends NTSC signals captured from the video camera at 5.685GHz uninterruptedly during the experiment. In the first part of the experiment the receiver base was rotated from $-90°$ to $+90°$ every $10°$ with the help of a protractor as shown in Figure 3.5 while keeping the transmitter base unchanged. The receiver base was rotated instead of changing the transmitter position for practicality reasons. This step is important to verify the estimation accuracy in a static situation. Data was captured for approximately 20 seconds for every receiver base position. Later on, the real-time experiment was held, in which the receiver base was continuously rotated and estimation processing was concomitantly made. Following the data acquisition step, the post-processing of the static experiment was performed to calculate the estimation of the direction of arrival of each step of the rotation of the receiver base.

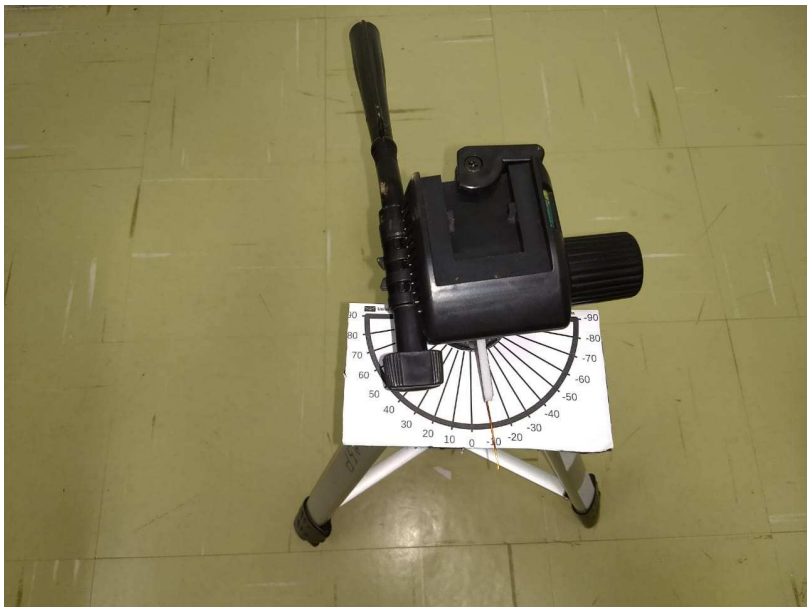

Figure 3.5: Protractor used to verify the rotation of the receiver base. There is a precision error that becomes larger for larger values of $|\theta|$.

3.3 RSSI Calibration

The AD9361 measures the received signal strength indicator (RSSI) by measuring the power level in dB and compensating for the receive path gain. Equating the RSSI read-back value to an absolute power level (e.g., in dBm) requires a system factory or bench calibration. To calibrate the RSSI word to an absolute reference, a signal was injected into the antenna port of the AD-FMCOMMS5-EBZ board and the RSSI word was read with a spectral analyzer. Subsequently, a correction factor that equates the RSSI word to the injected signal level at the antenna port was generated. The result of this calibration process is shown in Figure 3.6, where the blue dots are the measured points and the red line is the linear approximation.

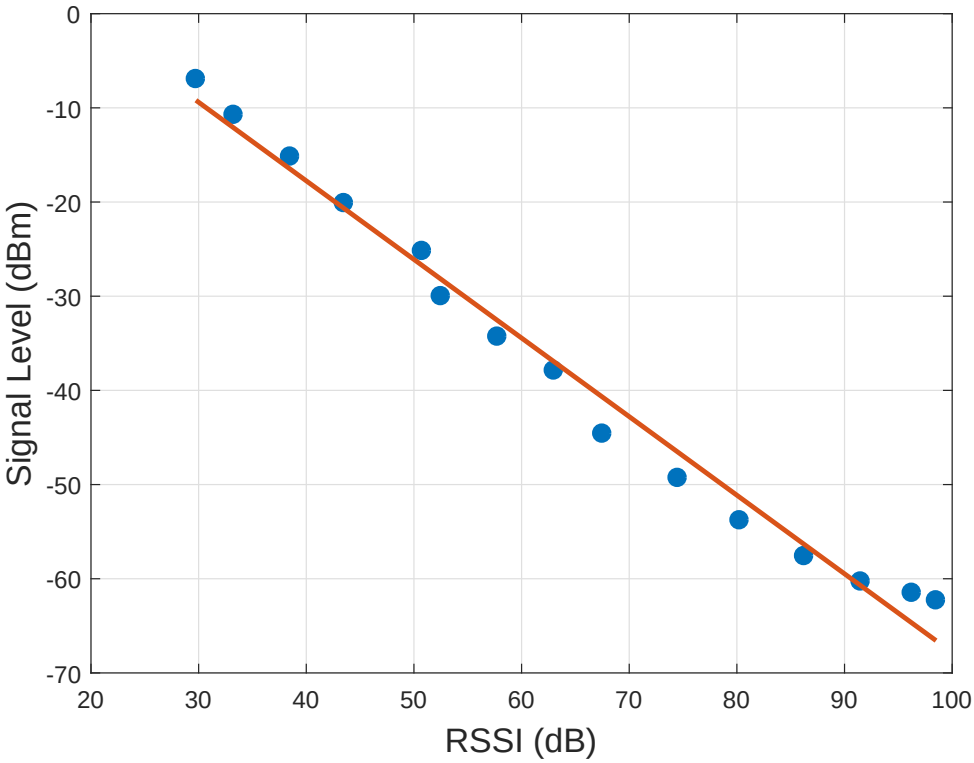

Figure 3.6: Calibration of the RSSI value into a signal level in dBm.

The input signal generated by the AD-FMCOMMS5-EBZ was a 100Hz sine function modulated at a frequency of 5.685GHz. This signal was injected in the same board to verify the correspondent RSSI value. Subsequently, the signal was injected in the spectral analyzer to verify the correspondent signal power in dBm. The power of the sine wave was regulated by modifying the attenuation value of the board output. By doing this repeatedly for different attenuation values, the graph in Figure 3.6 was plotted. Some examples of this procedure can be observed in Figure 3.7. As seen in Figure 3.7(a) and 3.7(b), for an attenuation of 20dB, the RSSI value measured with the board is 51dB, and the signal level read by the spectral analyzer is -25.05dBm.

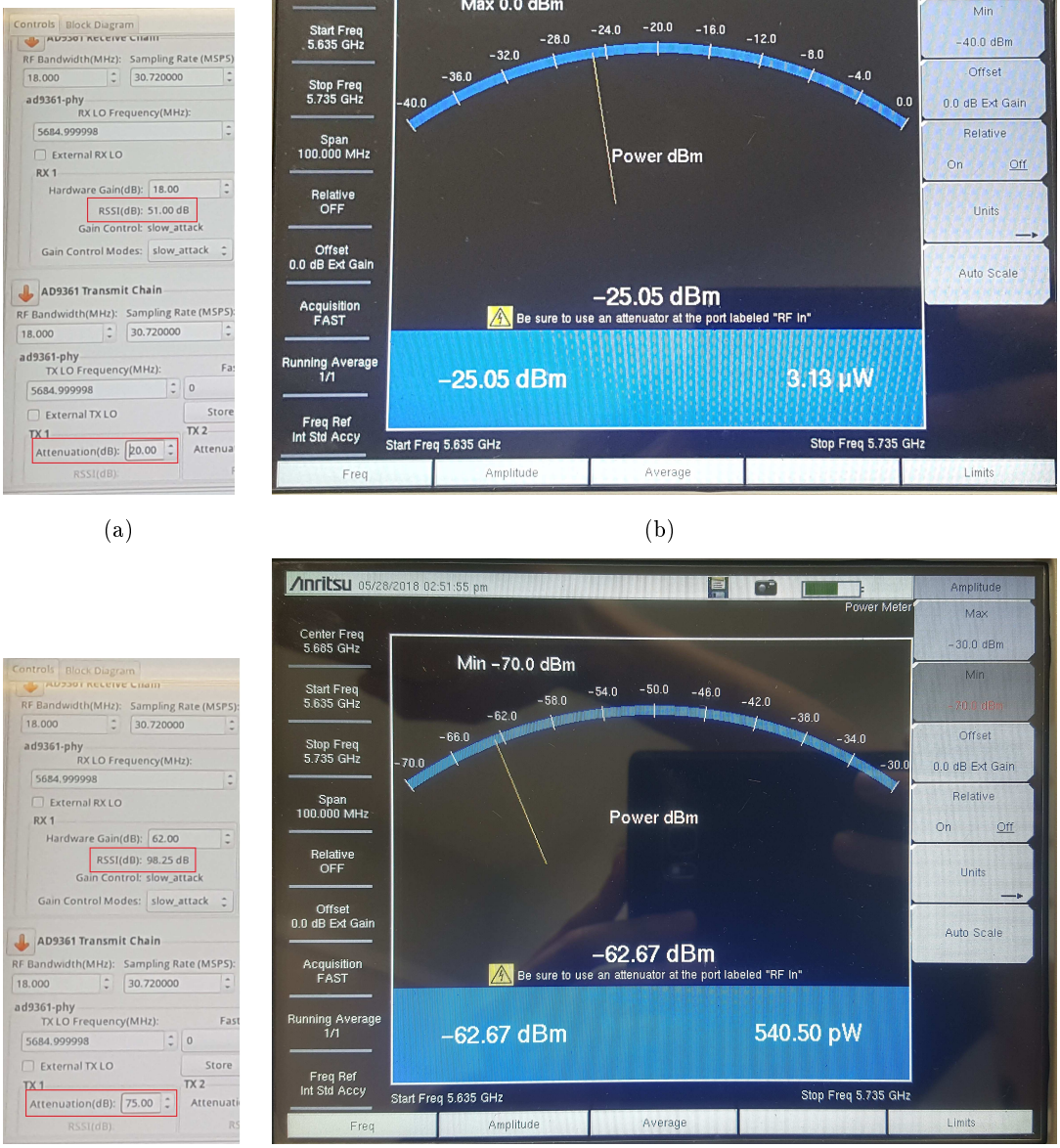

Figure 3.7: Received signal strength indicator calibration.

The calibration equation that relates the RSSI value to an absolute reference in dBm is:

$$y[\text{dBm}] = f(x) = -0.8345x + 15.6296, \tag{3.1}$$

where x is the RSSI signal level in dB. This equation is used just after the RSS measurements with the AD9361 to obtain power levels in dBm, which are subsequently used to calculate the direction of arrival.

3.4 Results and Analysis

In this section a descriptive analysis of the results obtained after processing the data acquired during the field experiments is held.

Table 3.2: Mean and variance of the DoA estimation values and their respective absolute error

θ	$\mathrm{E}[\hat{\theta}]$	$\mathrm{Var}[\hat{\theta}]$	$\mathrm{E}[\lvert\theta - \hat{\theta}\rvert]$	$\mathrm{Var}[\lvert\theta - \hat{\theta}\rvert]$
$-90°$	$57.37°$	$438.54°$	$34.61°$	$299.94°$
$-80°$	$-60.45°$	$110.23°$	$21.04°$	$48.59°$
$-70°$	$-65.38°$	$37.52°$	$6.74°$	$12.96°$
$-60°$	$-65.59°$	$10.84°$	$6.31°$	$2.09°$
$-50°$	$-45.55°$	$0.46°$	$4.45°$	$0.46°$
$-40°$	$-40.34°$	$3.26°$	$1.40°$	$1.37°$
$-30°$	$-34.77°$	$8.34°$	$4.98°$	$6.27°$
$-20°$	$-22.77°$	$0.47°$	$2.77°$	$0.47°$
$-10°$	$-5.31°$	$0.15°$	$4.69°$	$0.15°$
$0°$	$-3.89°$	$0.47°$	$3.89°$	$0.47°$
$+10°$	$12.59°$	$0.16°$	$2.59°$	$0.16°$
$+20°$	$19.98°$	$0.23°$	$0.41°$	$0.06°$
$+30°$	$16.41°$	$1.96°$	$13.59°$	$1.96°$
$+40°$	$46.65°$	$13.03°$	$6.65°$	$13.03°$
$+50°$	$90.46°$	$0.08°$	$40.46°$	$0.08°$
$+60°$	$64.23°$	$132.53°$	$6.57°$	$106.70°$
$+70°$	$69.74°$	$81.62°$	$7.55°$	$23.59°$
$+80°$	$58.52°$	$59.00°$	$21.48°$	$59.00°$
$+90°$	$82.22°$	$323.83°$	$4.38°$	$35.37°$

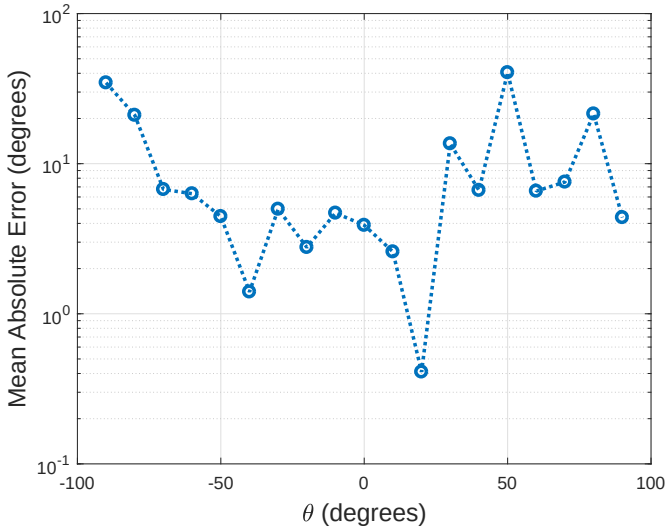

Figure 3.8: Plot of the mean absolute error $\mathrm{E}[|\theta - \hat{\theta}|]$.

The mean and variance in Table 3.2 were taken over 10 seconds of RSSI measurements. The plot of the third column of the same table, representing the mean absolute error, is shown in Figure 3.8. From Figure 3.8 it is noticeable that the average absolute estimation error of the direction of arrival was less than 10° for most cases of direction of arrival. This result was achieved after processing and calibrating the DoA estimation algorithm. In the next paragraphs I will analyze the not precise estimation results and show how the calibration was performed.

To analyze the source of error of the DoA estimations, it is important to observe Figure 3.9, where the order of the RSS values in each antenna for a correct DoA estimation is shown. To obtain good estimations it is necessary for the RSS values to follow the same order as shown in Figure 2.2(b), because when the vectors $\mathbf{p}(\theta)$ and $\mathbf{g}(\theta)$ are computed (see section 2.4), the algorithm analyzes the maximum points of the spatial power response $P(\theta)$ with Equations (2.9) and (2.12) (that is, the point with the least distance between $\mathbf{p}(\theta)$ and $\mathbf{g}(\theta)$) to calculate the estimation $\hat{\theta}$. The first source of error in the estimation comes from the computing of $P(\theta)$.

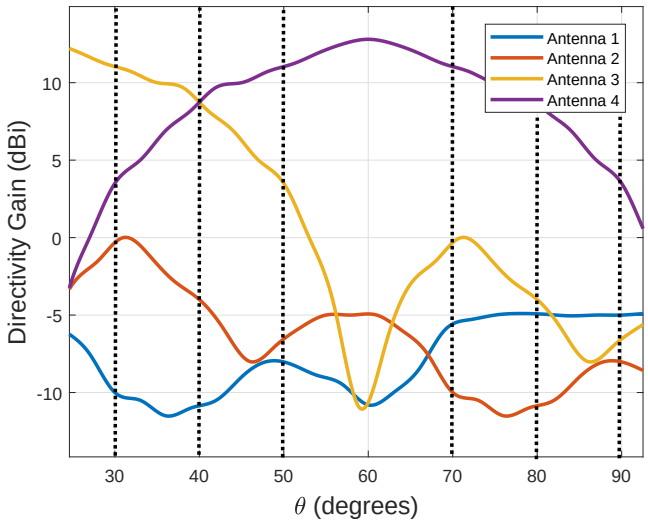

Figure 3.9: Array directivity gain pattern zoomed to highlight the points of $+30° \leq \theta \leq +90°$.

From this point, the DoA estimation for the cases $\theta = +90°$, $\theta = +80°$, $\theta = +70°$, $\theta = +50°$, $\theta = +40°$, and $\theta = +30°$ will be individually analyzed, since higher estimation error happened for all of them in a first deployment of the estimation algorithm. The same analysis can be extended to the cases $\theta = -90°$ and $\theta = -80°$.

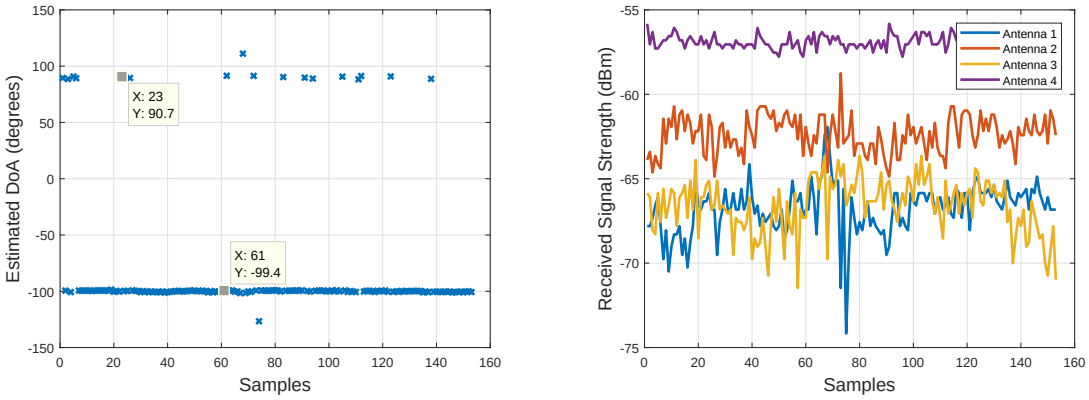

(a) (b)

Figure 3.10: (a) DoA estimation and (b) RSS measurements for $\theta = +90°$.

As it can be seen in Figure 3.10, although for most samples of RSS the direction of arrival is estimated as approximately equal to $-100°$, that is, there is an absolute estimation error close to $180°$, there are some samples in which their DoA estimation $\hat{\theta}$ is close to $+90°$ with an average absolute error less than $2°$, which is a precise result. By looking at Figure 3.10(b) the highest RSS value is read at antenna 4, which is in accordance with expectation as seen in Figure 3.9. The precise DoA estimation occurred when the RSS values read by antennas 1, 2, and 3 are close to each other. However, the possible source of DoA estimation error lies in the RSS value read at antenna 2. One can notice that this value is the second highest one at the array after antenna 4,

when it should actually be the lowest one, according to Figure 3.9.

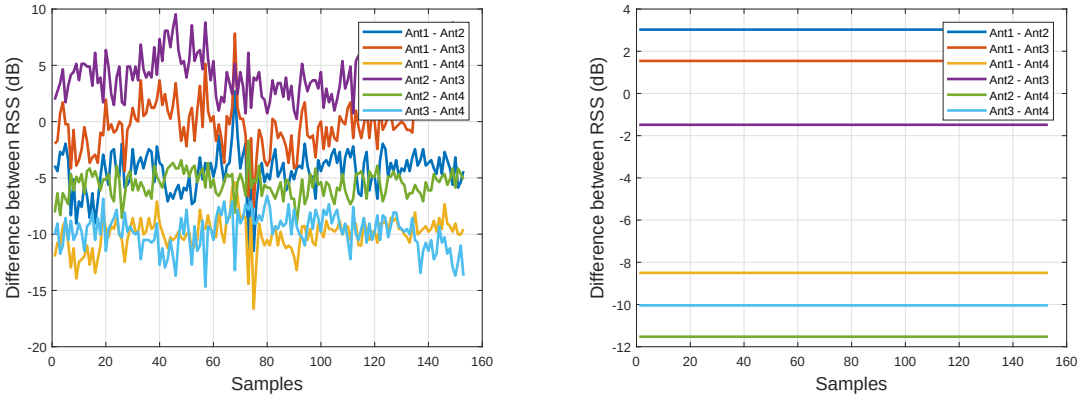

(a) (b)

Figure 3.11: (a) Measured RSS differences and (b) expected gain differences for $\theta = +90°$. Only the double differences are considered for simplicity in the analysis.

The present analysis is further facilitate with Figure 3.11. The RSS difference between each antenna (see Equations (2.7) and (2.8)) is shown in Figure 3.11(a), and the directivity gains difference between each antenna (see Equations (2.10) and (2.11)) is shown in Figure 3.11(b). By comparing both figures it is concluded that the RSS at antenna 2 is the reason of a high absolute estimation error. If the RSS at antenna 2 is ignored during the DoA estimation, the result obtained is shown in Figure 3.12.

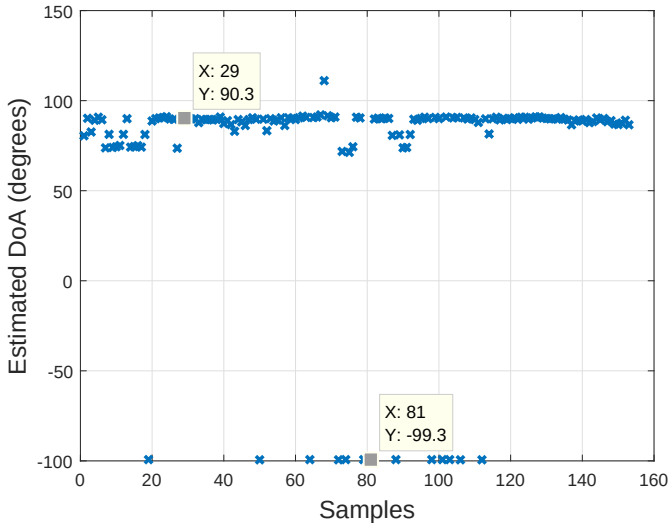

Figure 3.12: DoA estimation for $\theta = +90°$ without considering the RSS at antenna 2.

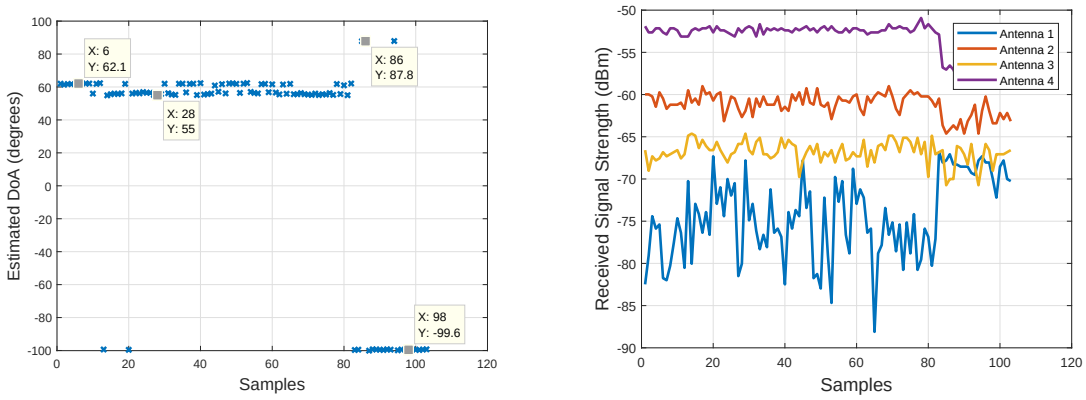

(a) (b)

Figure 3.13: (a) DoA estimation and (b) RSS measurements for $\theta = +80°$.

The $\theta = +80°$ case will now be analyzed. If the samples having high estimation error are excluded, on average the estimated DoA $\hat{\theta}$ is approximately $+60°$, with an average absolute estimation error of $20°$. By analyzing the RSS at each antenna in Figure 3.13(b), again the values read at antenna 2 are one of the causes for the estimation error. Another possible cause is the RSS at antenna 1, that is on average lower than expected. Repeating the procedure made for the $\theta = +90°$ case without considering the RSS at antenna 2, the obtained result is shown in Figure 3.14. It is noticeable that the estimation is overall better, but still not too precise.

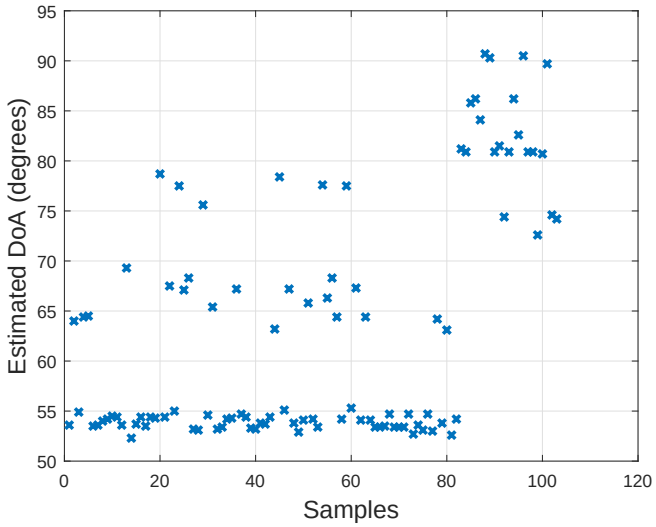

Figure 3.14: DoA estimation for $\theta = +80°$ without considering the RSS at antenna 2.

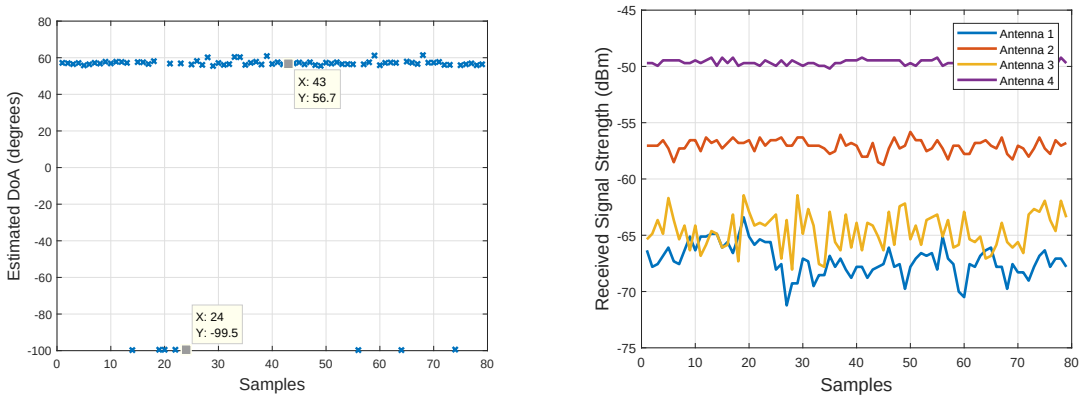

(a) (b) $\theta = +70°$

Figure 3.15: (a) DoA estimation and (b) RSS measurements for $\theta = +70°$.

The RSS at antenna 2 is again affecting the DoA estimation for the $\theta = +70°$ case as shown in Figure 3.15. Repeating the same procedure of excluding the RSS at antenna 2 as before, the following result is obtained, as shown in Figure 3.16. Again the result is overall better than before.

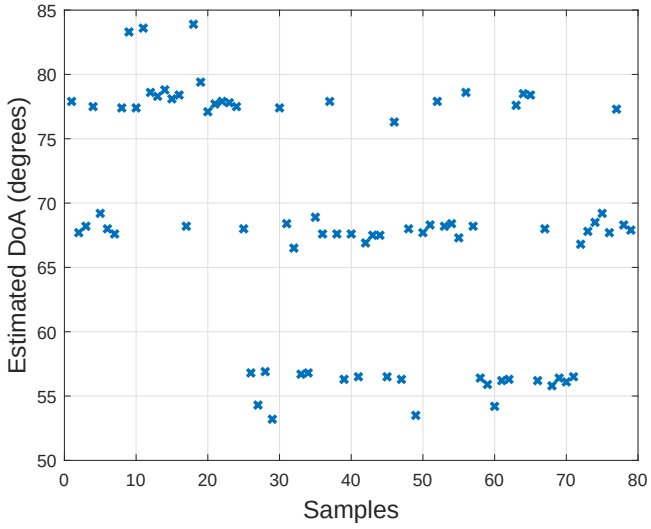

Figure 3.16: DoA estimation for $\theta = +70°$ without considering the RSS at antenna 2.

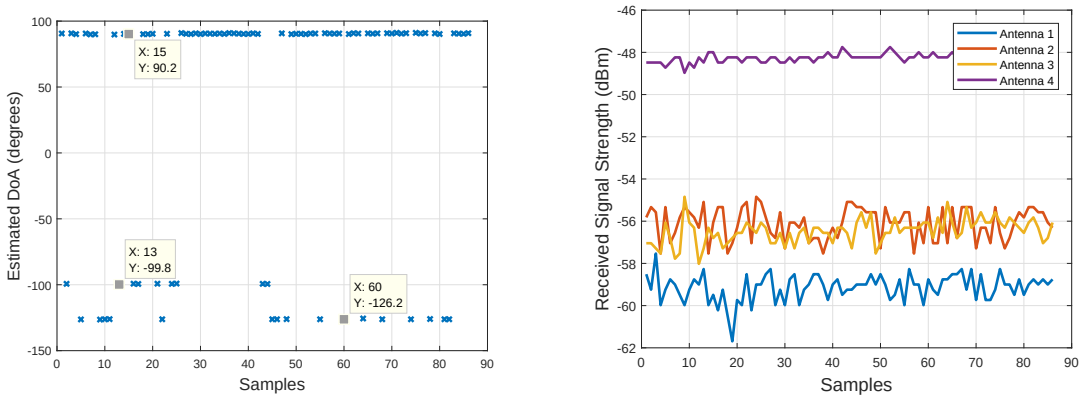

(a) (b)

Figure 3.17: (a) DoA estimation and (b) RSS measurements for $\theta = +50°$.

The $\theta = +50°$ case is the one with the worse DoA estimation. If one compare Figure 3.17(b) with Figure 3.9, one can notice that it is expected that the RSS at antennas 1 and 2 should be close to each other while the RSS at antenna 3 should be higher than them. However, this is not what happens in practice, where the measured RSS at antennas 2 and 3 are roughly close to each other while the RSS at antenna 1 is the lowest one. Once more it is possible that the measurements at antenna 2 is degrading the DoA estimation. To confirm the cause of the present estimation error, the measured RSS differences and expected directivity gain differences are showed in Figure 3.18.

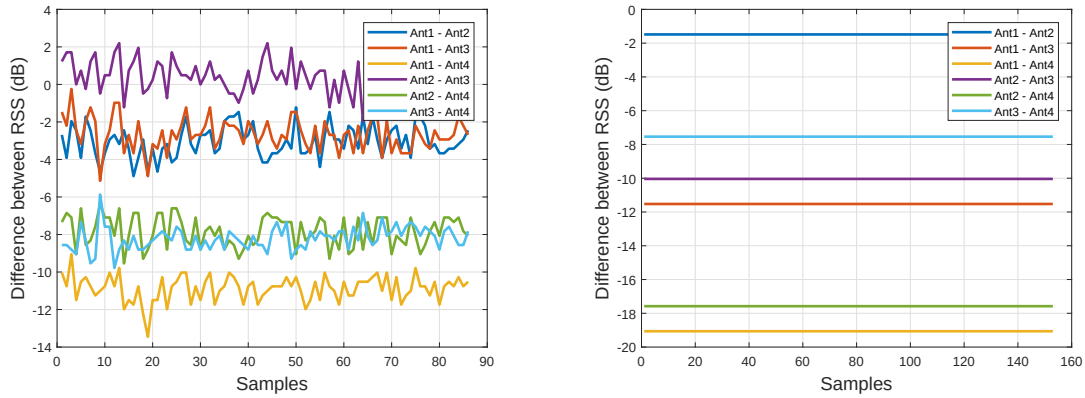

(a) (b)

Figure 3.18: (a) Measured RSS differences and (b) expected gain differences for $\theta = +50°$. Only the double differences are considered for simplicity in the analysis.

From Figure 3.18(a) one can see that the measurements at all four antennas are opposed to the expected ones as in Figure 3.18(b). The same error is not observed for the opposite case of $\theta = -50°$ as shown in Figures 3.19 and 3.20.

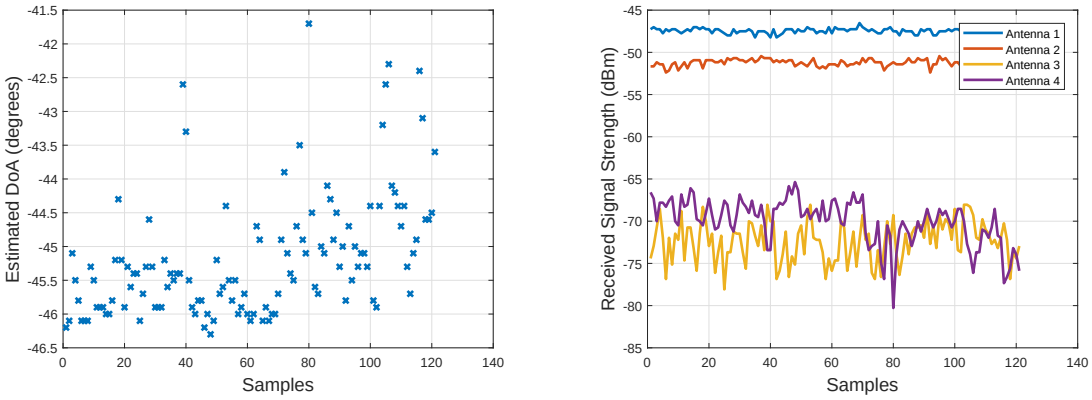

(a) (b)

Figure 3.19: (a) DoA estimation and (b) RSS measurements for $\theta = -50°$.

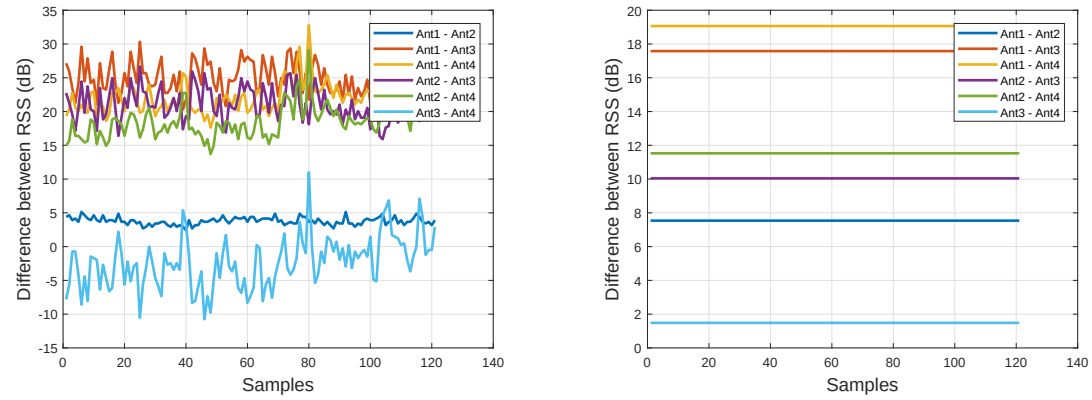

(a) (b)

Figure 3.20: (a) Measured RSS differences and (b) expected gain differences for $\theta = -50°$. Only the double differences are considered for simplicity in the analysis.

The discussion now is for the $\theta = +40°$ case. As observed in Figure 3.21(a) the DoA estimation for this case was precise for most collected RSS samples, with an average error less than 7°. However, since there are some really not precise estimation points, the mean absolute error was high, as shown in Table 3.2. By comparing Figure 3.21(b) with Figure 3.9 there is a point around $+46°$ where the RSS at antennas 1 and 2 are close to each other, explaining the estimation at this point, since most collected RSS samples present this pattern. However, there are also some points where the RSS at antenna 2 is too low, contradicting the expected pattern and thus affecting a correct estimation. If a filter is applied to the output of the DoA estimator to cut off the high error estimation points, the average estimation accuracy will increase.

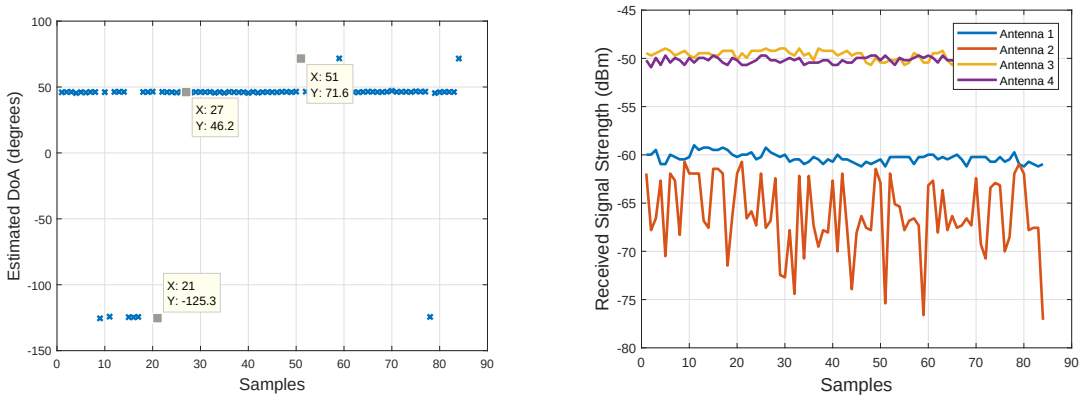

(a) (b)

Figure 3.21: (a) DoA estimation and (b) RSS measurements for $\theta = +40°$.

Lastly, the analysis is directed to the $\theta = +30°$ case. Again it is observable that the RSS at antenna 2 was lower than that of antenna 1, thus affecting the estimation. Since the opposite case $\theta = -30°$ does not present a similar estimation error (see Figure 3.23), it is possible that there is either a hardware error that is affecting the RSS measurements at the antennas or magnetic coupling is causing a distortion in the directional antennas sidelobes.

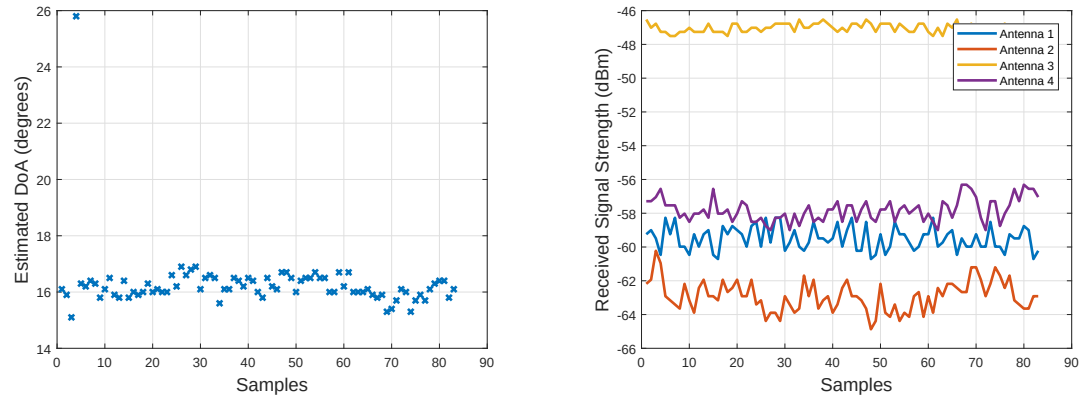

(a) (b)

Figure 3.22: (a) DoA estimation and (b) RSS measurements for $\theta = +30°$.

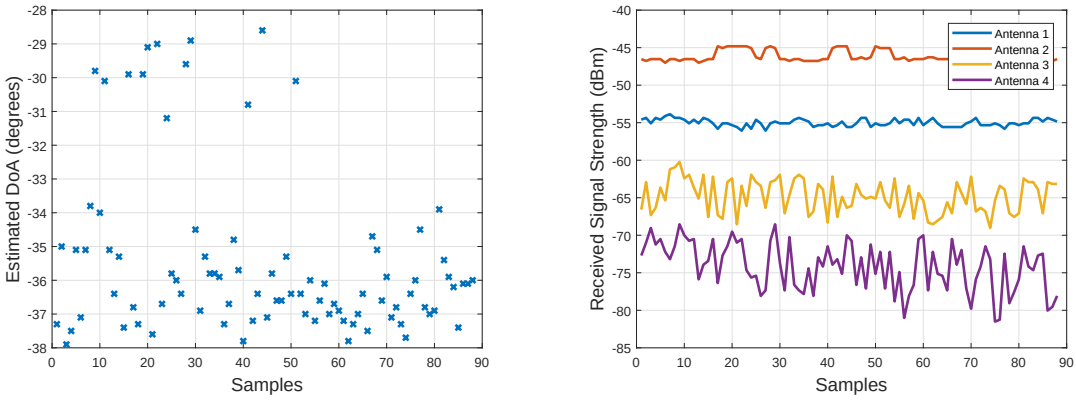

(a) (b)

Figure 3.23: (a) DoA estimation and (b) RSS measurements for $\theta = -30°$.

Concluding, the side lobes of the directional antennas are not behaving as theoretically expected for all the cases with high estimation error. Possible reasons for this is either the mutual coupling between the antennas, which was not considered in the development of the technique proposed in this work, or hardware issues.

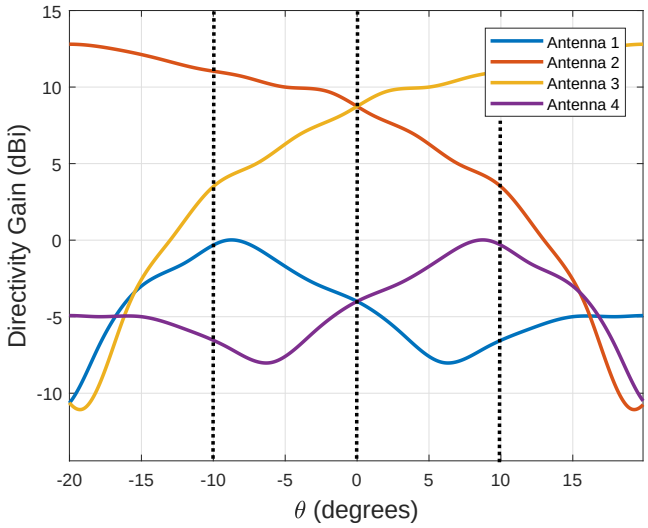

Figure 3.24: Array directivity gain pattern zoomed to highlight the points of $-20° \leq \theta \leq +20°$.

The discussion now is for Figures 3.24 and 3.25, where the latter depicts the $\theta = -10°$, $0°$, and $+10°$ cases. The analysis will be focused on only these three cases because a good precision estimation $\hat{\theta}$ was achieved and all other cases follows the same idea. Since all RSS measurements were accordingly to the theoretical model as shown in Figure 3.24, the estimation was also precise, with an average absolute error less than 5°. If the receiver base was rotated more precisely during the experiment, it is possible that the estimation results would have been more accurate. Therefore, the precision in the base rotation also accounts for the final estimation error. After some simple

measurements, it was found that this precision is about 3°, thus the averaged absolute errors in Table 3.2 for $\theta = -10°$, 0°, and $+10°$ should be subtracted by this value. The precision gets worse for larger values of $|\theta|$.

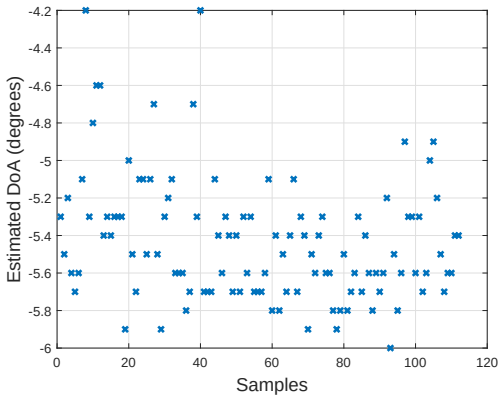

(a) $\theta = -10°$

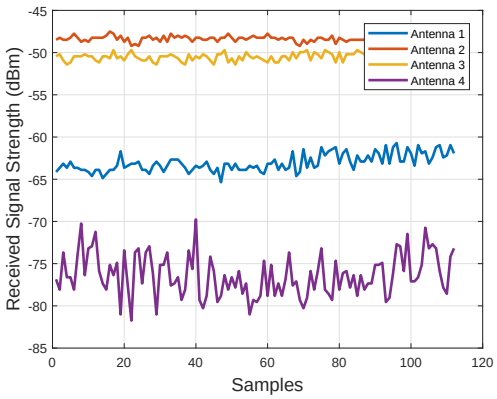

(b) $\theta = -10°$

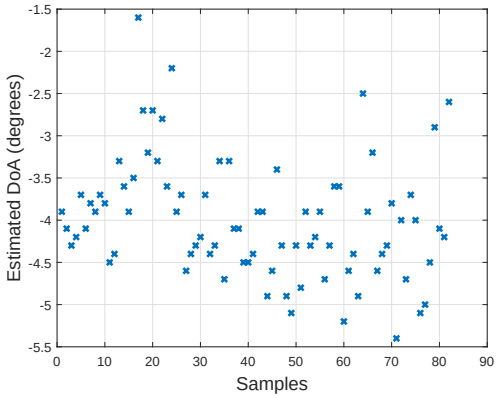

(c) $\theta = 0°$

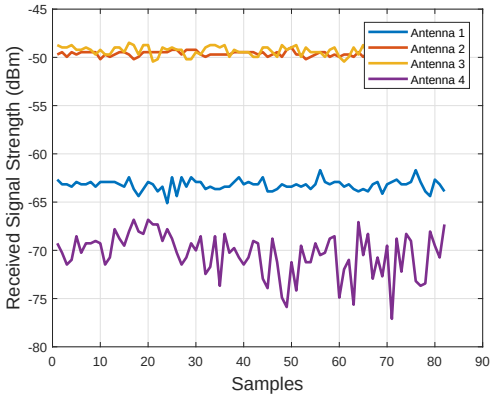

(d) $\theta = 0°$

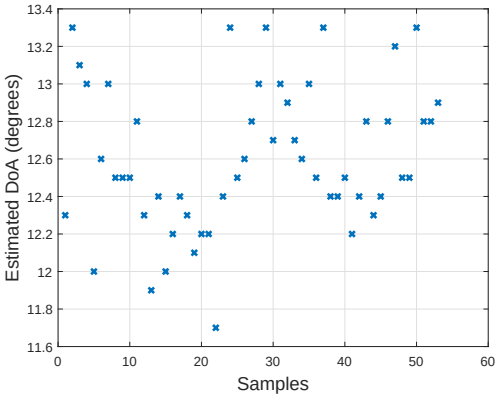

(e) $\theta = +10°$

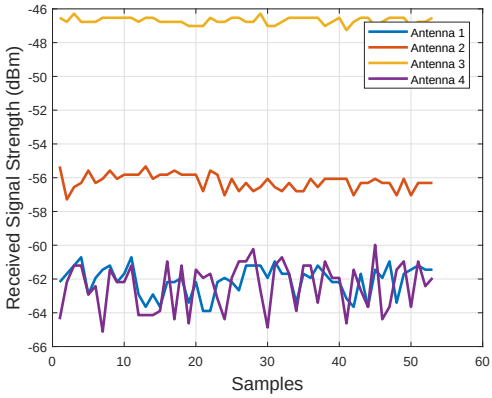

(f) $\theta = +10°$

Figure 3.25: DoA estimation and RSS measurements for values of θ with a more precise estimation.

3.4.1 Realtime Field Experiments

The discussion now is about the realtime field experiment, where the direction of arrival of the NTSC transmitter was estimated in realtime while rotating the receiver base, starting from the position where the antenna 1 is pointing to the direction of the transmitter ($\theta = -90°$). In Figure 3.26 the results of this experiment are shown.

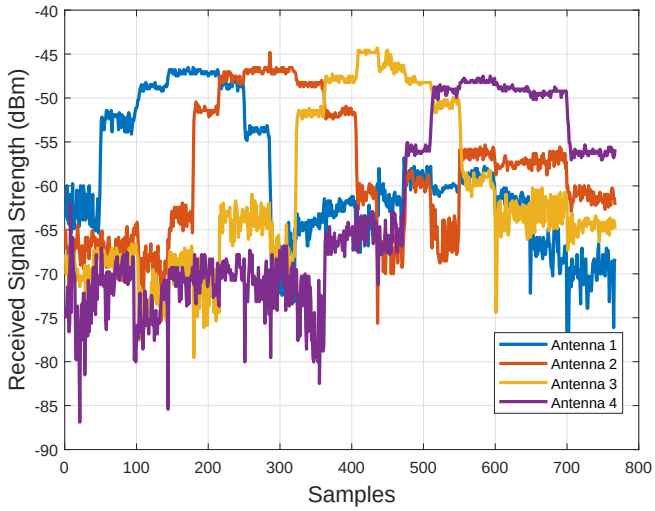

(a) Received signal strength in each antenna

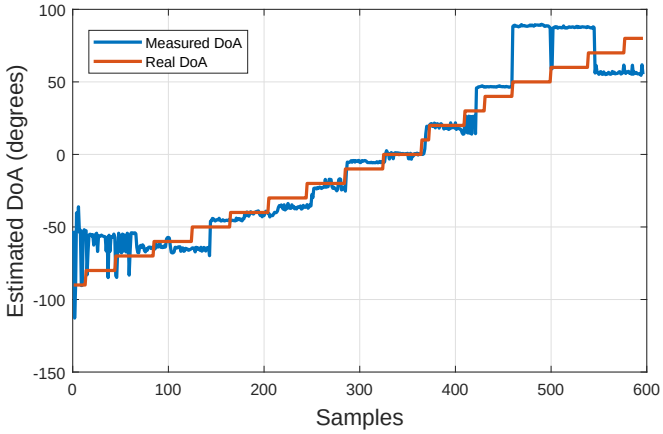

(b) Estimated DoA

Figure 3.26: Realtime DoA experiment.

Theoretically, the graph in Figure 3.26(b) should resemble an increasing step-like function graph, from $-90°$ to $+90°$ as shown with the orange line. The absolute estimation error is depicted in Figure 3.27(a).

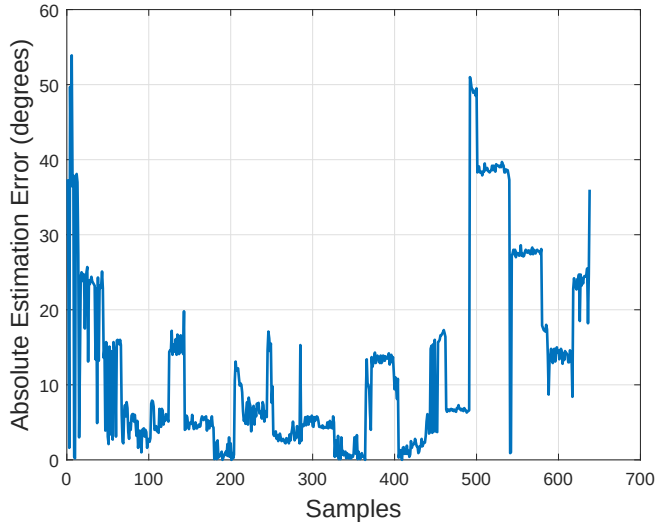

(a)

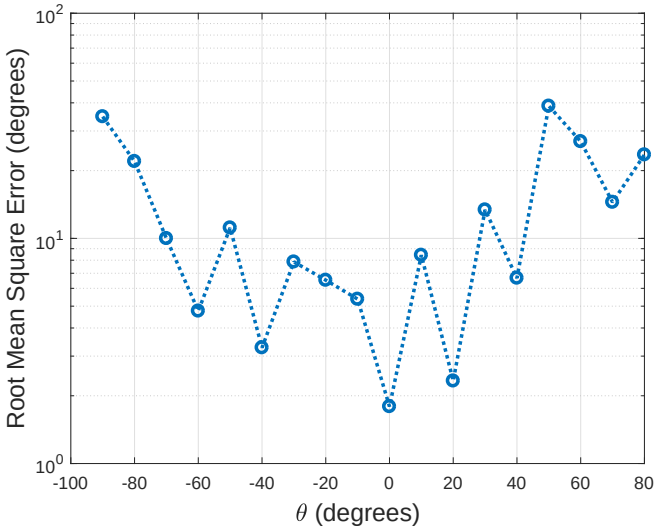

(b)

Figure 3.27: (a) Absolute estimation error for the realtime DoA experiment. (b) Root mean square error of (a).

By observing Figure 3.27(a) one can see that the absolute estimation error graph lies mostly under the 20° line. Ideally, this graph should be as close as possible to 0°, because it would mean that the absolute error was near to zero. If the RMSE is calculated, it can be seen from Figure 3.27(b) that a considerably precise estimation was achieved for values between $-70°$ and $+40°$, with an RMSE less than 10°. Otherwise, a less accurate $\hat{\theta}$ was obtained.

Another experiment was to show the realtime DoA estimation of a moving drone with the aid of gauges. The estimation was accurate between $\theta = -60°$ and $+60°$, when it was noticeable the concurrent movement of the needle of the gauge with the movement of the drone. However, less accurate estimation was obtained otherwise, with the needle either stopping moving on the

$|\theta| = 60°$ or pointing to wrong directions.

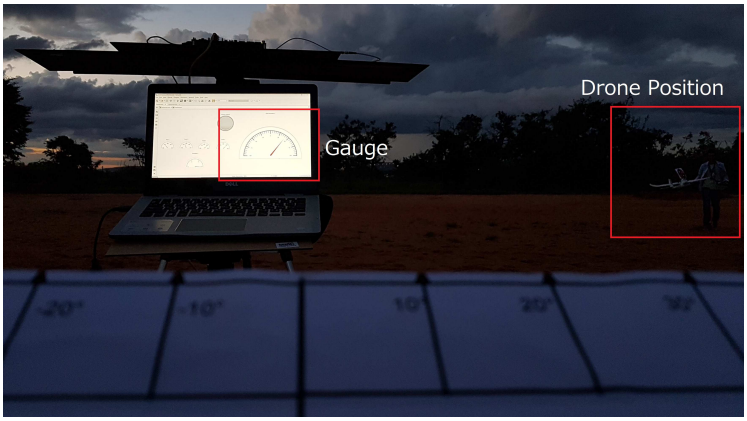

Figure 3.28: Gauge showing the estimated location of a moving drone. With the help of a plane protractor, it can be concluded that the estimation is precise (approximately $\hat{\theta} = 35°$).

Chapter 4

Conclusions and Future Work

The main purpose of this work was to develop an algorithm capable of estimating the direction of arrival of a transmitting source (UAV) based on the received signal strength at the directional antennas on an array, to calculate the optimum angular spacing ϕ_{opt} between the antennas, and to verify the efficacy and efficiency of the proposed technique with low-cost off-the-shelf equipment, such as the Yagi-Uda antennas and software-defined radio.

In Sections 2.2, 2.3, and 2.4 it was presented the fundamentals of the technique proposed in this work for UAVs localization. By computing the difference vector $\mathbf{p}(\theta)$ which contains both the double and quadruple differences between the received signal strengths of any antennas and then comparing it with the difference vector $\mathbf{g}(\theta)$ via Equation (2.9), the estimation of the direction of arrival $\hat{\theta}$ was calculated via the cost function (2.12). After analyzing the simulation results in Section 2.5 it was concluded that the optimum angular spacing ϕ_{opt} lies within the interval of 35° and 65° with a root-mean-square error less than 10°. We proved through simulation that the direction of arrival estimation technique presented in this work is efficient in the sense of localizing UAVs.

In Section 3.2 the equipments used during the field experiments and the methodology followed were described. The used equipments are the low-cost off-the-shelf devices such as the YE572113 Yagi-Uda antennas, AD-FMCOMMS5-EBZ board, and transmitter set. The cost of the equipment was approximately US$2000. A brief description of all devices were also presented. Since the hardware used for the reception of the NTSC signal provides the power level of an input signal in its ports in dB (received signal strength indicator), calibrating it to an absolute power level in dBm became needed for further computing of the estimation algorithm. In Section 3.3 the calibration process and its methodology is described. It is shown that, the larger the RSSI power level in dB, the weaker is the signal (that is, small power level in dBm). The results obtained after field experiments are analyzed in Section 3.4. From table 3.2 the technique appears to be appropriate for most values of the transmitter position θ after calibration. However, before calibration the estimation was satisfactory for few positive values of θ. The technique to enhance the estimation for these values is also detailed. After analyzing the received signal strength and their double differences at each antenna for the unsatisfactory cases, it is thought that the first reason of

estimation inaccuracy is the distorted side lobes of the pattern of the directional antennas, caused possibly by magnetic coupling between them.

To further enhance the precision of the present DoA estimation algorithm and also possibly reduce costs some points need to receive attention.

- **Calibration of the hardware and antennas**. Although the present work was mostly plug-and-play, better results are expected if a thorough calibration of the hardware is performed. The receiving gain of the hardware in use and the antennas bandwidth, for example, must be taken into account.

- **Measurements of the array gain pattern inside an anechoic chamber**. The directivity gain pattern of one directional antenna was simulated from the measurements supplied by the manufacturer in the YE572113 antenna datasheet. Then, the array pattern was computed by only shifting a single pattern without considering mutual coupling between the antennas. For this reason, precise measurements of the gain pattern of the array should be done inside an anechoic chamber. In so doing, it is believed that the accuracy in the estimation though Equation (2.9) becomes better since the measured RSS values will be compared with the actual array gain pattern;

- **Number of antennas used on the array**. It is helpful to know how the number of antennas on the array affect the overall estimation algorithm. By reducing the number of antennas, rotating them around their common axis and saving the corresponding gain pattern, the vector $\mathbf{g}_{\text{array}}(\theta)$ will possibly not suffer any changes. Thus, the same technique could be applied with less antenna elements;

- **Simulating the noise n (see Section 2.2)**. The noise present in the channel should be included during the simulation to verify its effect on the overall estimation precision;

- **Controlling the transmitter side**. The transmitter sends NTSC signal uninterruptedly. However, this side of the communication channel should also be controlled in order to investigate other performance parameters such as the bit error rate (BER). Instead of an analog signal such as the NTSC, a digital signal with an appropriate modulation and demodulation scheme ought to be tested;

- **Estimating the DoA with other techniques**. A comparison of the presented DoA estimation technique with others is also encouraged. For example, the authors in [21] propose a DoA estimation algorithm based on the Capon algorithm for the use with directional antennas array. The traditional MUSIC and MLE techniques should also be verified;

- **Calculation of other parameters**. When the estimated DoA $\hat{\theta}$ is found, other parameters such as the distance R between transmitter and receiver can also be estimated by means of the Friis Transmission Equation (see Eq. (2.1);

- **Calculation of the Cramer-Row Bound (CRB)**;

BIBLIOGRAPHIC REFERENCES

[1] ECONOMIST, T. *TECHNOLOGY QUARTERLY TAKING FLIGHT*. Disponível em: <https://www.economist.com/technology-quarterly/2017-06-08/civilian-drones>.

[2] FORTUNE. *This Might Be the First Drone-Related Aircraft Crash*. feb 2018. Disponível em: <http://fortune.com/2018/02/16/south-carolina-drone-helicopter-crash/>.

[3] ALEXIOU, A.; HAARDT, M. Smart antenna technologies for future wireless systems: trends and challenges. *IEEE Communications Magazine*, v. 42, n. 9, p. 90–97, Sept 2004. ISSN 0163-6804.

[4] MARINHO, M. A. et al. Robust nonlinear array interpolation for direction of arrival estimation of highly correlated signals. *Signal Processing*, v. 144, p. 19 – 28, 2018. ISSN 0165-1684. Disponível em: <http://www.sciencedirect.com/science/article/pii/S016516841730347X>.

[5] MIRANDA, R. K. et al. Broadband beamforming via frequency invariance transformation and parafac decomposition. In: *2017 IEEE 7th International Workshop on Computational Advances in Multi-Sensor Adaptive Processing (CAMSAP)*. [S.l.: s.n.], 2017. p. 1–5.

[6] ZANATTA, M. da R. et al. Antenna array based receivers for third generation global positioning system. In: *2017 Workshop on Communication Networks and Power Systems (WCNPS)*. [S.l.: s.n.], 2017. p. 1–4.

[7] MARANHAO, J. P. A. et al. Antenna array based framework with multipath mitigation for signal emitter detection and localization. In: *2017 11th International Conference on Signal Processing and Communication Systems (ICSPCS)*. [S.l.: s.n.], 2017. p. 1–5.

[8] SANUDIN, R. et al. Analysis of doa estimation for directional and isotropic antenna arrays. In: *2011 Loughborough Antennas Propagation Conference*. [S.l.: s.n.], 2011. p. 1–4.

[9] CHEN, Z.; GOKEDA, G.; YU, Y. *Introduction to Direction-of-Arrival Estimation*. [S.l.]: Artech House, 2010.

[10] KRIM, H.; VIBERG, M. Two decades of array signal processing research: the parametric approach. *IEEE Signal Processing Magazine*, v. 13, n. 4, p. 67–94, Jul 1996. ISSN 1053-5888.

[11] ZISKIND, I.; WAX, M. Maximum likelihood localization of multiple sources by alternating projection. *IEEE Transactions on Acoustics, Speech, and Signal Processing*, v. 36, n. 10, p. 1553–1560, Oct 1988. ISSN 0096-3518.

[12] MUHAMED, R.; RAPPAPORT, T. S. Comparison of conventional subspace based doa estimation algorithms with those employing property-restoral techniques: simulation and measurements. In: *Proceedings of ICUPC - 5th International Conference on Universal Personal Communications*. [S.l.: s.n.], 1996. v. 2, p. 1004–1008 vol.2.

[13] ULUSKAN, S.; FILIK, T. Rss based direction finding via array of directional antennas with normal density distribution in magnitude. In: *2017 10th International Conference on Electrical and Electronics Engineering (ELECO)*. [S.l.: s.n.], 2017. p. 656–660.

[14] KULAS, L. Rss-based doa estimation using espar antennas and interpolated radiation patterns. *IEEE Antennas and Wireless Propagation Letters*, v. 17, n. 1, p. 25–28, Jan 2018. ISSN 1536-1225.

[15] TAILLEFER, E.; HIRATA, A.; OHIRA, T. Direction-of-arrival estimation using radiation power pattern with an espar antenna. *IEEE Transactions on Antennas and Propagation*, v. 53, n. 2, p. 678–684, Feb 2005. ISSN 0018-926X.

[16] JIANG, J. R. et al. Alrd: Aoa localization with rssi differences of directional antennas for wireless sensor networks. In: *International Conference on Information Society (i-Society 2012)*. [S.l.: s.n.], 2012. p. 304–309.

[17] HOOD, B. N.; BAROOAH, P. Estimating doa from radio-frequency rssi measurements using an actuated reflector. *IEEE Sensors Journal*, v. 11, n. 2, p. 413–417, Feb 2011. ISSN 1530-437X.

[18] LIE, J. P.; BLU, T.; SEE, C. M. S. Single antenna power measurements based direction finding. *IEEE Transactions on Signal Processing*, v. 58, n. 11, p. 5682–5692, Nov 2010. ISSN 1053-587X.

[19] STUTZMAN, W. L.; THIELE, G. A. *Antenna Theory and Design*. [S.l.]: Wiley, 2012.

[20] CIDRONALI, A. et al. Analysis and performance of a smart antenna for 2.45-ghz single-anchor indoor positioning. *IEEE Transactions on Microwave Theory and Techniques*, v. 58, n. 1, p. 21–31, Jan 2010. ISSN 0018-9480.

[21] SANUDIN, R. et al. Capon-like doa estimation algorithm for directional antenna arrays. In: *2011 Loughborough Antennas Propagation Conference*. [S.l.: s.n.], 2011. p. 1–4.